1 **More trees, more rain? The unexpected role of forest and aquifers on the global water cycle**
2
3 Jean Chéry[1], Michel Peyret[1], Cédric Champollion[1] and Bijan Mohammadi[2]
4
5 [1] Geosciences Montpellier, Montpellier University, France
6 [2] Institut de Mathématiques Alexandre Grothendieck, Montpellier University, France
7
8 Corresponding author: Jean Chéry, e-mail: jean.chery@umontpellier.fr
9

10 **Abstract**
11
12 Forests' influence on rainfall has been debated since antiquity, with historical observations suggesting
13 that deforestation reduces precipitation. While early scientists believed that forests attract rain, later
14 research provided conflicting views, and modern climate models remain inconclusive on forests' role in
15 regional precipitation at continental scale. A difficulty of global climate model is the need to integrate
16 processes associated to multiple scientific field, like meteorology, hydrology and forest ecology. As a
17 result, the numerous constitutive equations, the complexity of numerical codes and the variability of
18 natural situations make difficult to provide a quantitative water cycle model controlled by a small
19 number of key parameters. Assuming water mass conservation between ocean, atmosphere, ecosphere
20 and continental aquifers, we revisit this problem and we build a simplified physical scheme of water
21 transfer across these reservoirs. Assembling a limited number of constitutive equations into a numerical
22 code, we propose a parsimony model able to simulate rainfall distribution patterns. Starting from initially
23 different vegetation conditions (sparse and dense), we identify the parameters modulating steady state
24 continental precipitation for both situations. First, we show that sparse vegetation patterns do not lead
25 to uniform and large continental precipitation. Rather, continental moisture is spatially limited by
26 atmospheric dispersion and wind, thus providing a decay of precipitation as a function of coastal distance
27 as observed in most cases worldwide. Second, our model predicts that large and widespread continental
28 precipitation results from the combination of dense vegetation patterns and deep aquifers low hydraulic
29 conductivity. This ecological/hydrological interaction is due to the slowness of horizontal water flow,
30 allowing underground reservoir level to increase enough for reaching plant roots, inducing in turn
31 vegetation evapotranspiration and atmospheric moisture. Overall, our model shed new light on the
32 balance between atmospheric water vapor transport by wind and dispersion, vegetation
33 evapotranspiration and underground water flow. Noticeably, the efficiency of the water cycle and its
34 related precipitation distribution not only depends from atmospheric parameters but is also largely
35 modulated by vegetation dynamics and underground aquifers behavior. We finally discuss how forest
36 growth or destruction may alter continental precipitation at various time scales.
37
38 "*Simplicity is the ultimate sophistication*" Leonardo da Vinci
39
40 "*In philosophy, Occam's razor (novacula Occami) is the problem-solving principle that recommends*
41 *searching for explanations constructed with the smallest possible set of elements. It is also known as*
42 *the principle of parsimony or the law of parsimony.*"
43 From Wikipedia
44
45 **1. Introduction**
46
47 <u>1.1 Historical background</u>
48
49   The possible influence of forests on the amount of precipitation has been debated since the Greek
50 Antiquity (Andréassian, 2004). Later, Christopher Columbus' son Fernando has related that his father
51 knew "*from experience*" that the disappearance of the forest that originally covered the Canary Islands,
52 Madeira and the Azores had reduced fog and rainfall. Likewise, he believed that the afternoon rains that
53 occur in Jamaica and the West Indies were the consequence of the islands "*lush forests*".

54   In 1787, Bernardin de Saint Pierre (cited in Descroix et al., 2001) notices about Mauritius island
55   in Indian Ocean that « *the vegetal attraction of the forests is so well matched by the metallic attraction*
56   *of the peaks of its mountains, that a field situated in an open area, in the neighbourhood, often lacks*
57   *rain, whereas it rains almost all year round in the woods which are not within rifle range*. » The idea
58   that forests attract and induce rain grew in France during the following decades and Dausse stated in
59   1842 that "*man has the power to change a wet climate into a dry one in just a few years by clearing*
60   *forests* ". Later in the 19th century, divergent views emerged and the opposite conclusion was reached
61   by Cézanne in 1872: "*forests cannot significantly alter the amount of rainwater that falls in a river*
62   *basin*" (also cited in Descroix et al., 2001).

63   Since the dawn of worldwide remote sensing, global scale data gathering and massive computing
64   meteorology, the vast amount of accumulated knowledge did not lead the scientific community towards
65   a clear understanding of the possible retroaction of forests on the regional annual precipitation at basin
66   scale. On the one hand, this diversity of opinion is not surprising because this scientific question
67   encompasses very different fields: theoretical physics, forestry, climatology, or/and hydrogeology.
68   Apart from fundamental chemistry and physics concepts, these communities share a limited common
69   knowledge, thus rendering difficult the building of an integrated vegetation / atmosphere / hydrosphere
70   / geosphere theory. On the other hand, this lack of agreement is somewhat intriguing nowadays because
71   forest / rain interaction is studied using advanced numerical climate packages in which most of relevant
72   constitutive equations are embedded, including all segments of continental water cycle: oceanic
73   evaporation, water vapor advection and transport to the continents, plant evapotranspiration and root
74   uptake, and ultimately water infiltration, deep storage and the way back to ocean by springs and rivers
75   (Gimeno at al. 2012).

76   Recently, the idea that forests induce rain gained new interest following the work of Makarieva
77   and Gorshkov (2007) (hereafter referred as MG2007). They propose that profiles, roughly perpendicular
78   to coastlines, across continents can be classified into two groups: (1) one shows a nearly constant
79   precipitation as a function of coastal distance in densely forested tropical and boreal areas, while (2)
80   another group displays a pronounced decay of rainfall from the coast towards inner continental zones
81   associated with bare soil or grasslands. MG2007 also propose a physical mechanism called "biotic
82   pump" explaining why forests are increasing pluviometry at regional scale. Briefly, the water vapor
83   induced by forest transpiration is prone to condensation during its adiabatic ascent in the lower
84   troposphere if convective conditions are met, leading to an atmospheric pressure drop over forested
85   areas. As a result, a pressure difference occurs between the inner continent and the overseas areas,
86   inducing a large-scale sea breeze importing moisture over forest that adds to the local moisture already
87   present, therefore increasing the precipitation probability. Major concerns also arose for the
88   sustainability of the Amazonian under hotter/drier climates and deforestation, with identified cascading
89   effects potentially leading to tipping points when climate/vegetation interactions will feed themselves
90   into an aridification spiral (Bochow and Boers, 2023; Sampaio et al., 2007; Wunderling et al., 2022)

91   Although the biotic pump explanation of MG2007 gained some popularity into scientific ecology
92   communities (Nobre, 2007; Sheil & Murdiyarso, 2009), the physical ground of this theory has been
93   disregarded by most climate modelling researchers. For example, Meesters et al. (2009) argued that the
94   physical approach of evaporation as provided by MG2007 was flawed and that high precipitation
95   occurring at sites located far from the ocean can be explained adequately by traditional theory, that
96   includes large scale advective processes (Coriolis forces, Hadley cells and monsoons), associated with
97   local re-evaporation process by the forest (Gimeno et al., 2012). Therefore, the dominant belief in
98   climate modeling research groups is that the effect of large forest over regional pluviometry is still
99   obscure (Douville et al., 2024).

100   While the capability of the forests to induce rain and change the meteorological regime over wide
101   continental areas remains an unsolved question, societal issues are raising under the pressure of
102   anthropogenic activities. First, the rise of average temperature since the beginning of the 20th century
103   increases evaporation of water bodies on land, the hydrologic pressure of underground waters and the
104   amount of evapotranspiration by forests. Therefore, if forests do not influence the precipitation regime,
105   their net effect negatively acts on water resources, suggesting that their expansion should be controlled

106 (Rambal, 2015; Asselin et al., 2024). Second, the amount of natural forests at global scale has been
107 decreasing for centuries (Hansen et al., 2013), due to the expansion of cultivated areas in developing
108 countries, widespread wood use (building and energy purposes among others), forest fires associated
109 with droughts or land use changes (Mouillot & Field, 2005). Third, the human water consumption is
110 increasing faster than the population growth (Serrano & Valbuena, 2017). The question of whether or
111 not large forests are our enemies (with pumping into hydrosystems and losing water vapor into the
112 atmosphere) or rather allies of mankind (in sustaining continental pluviometry) should be at the top of
113 many countries' agenda and a priority research program for international agencies. If the latter
114 hypothesis – postulating a positive forest influence on pluviometry – is correct, mankind will face a
115 negative feedback: continental water stock will unavoidably escape to ocean due to the syzygy of human
116 water consumption, global temperature rising and forested zones clearance (Steffen et al., 2015).

117 1.2 Need for a parsimony model
118
119 Why this question is not yet solved? A common answer could be that global water cycle,
120 continental pluviometry and forest ecology are controlled by many processes encompassing numerous
121 scientific fields, whose complexity and non-linearity render the associated mathematical problem non-
122 tractable, even for the most powerful codes (Vargas Godoy et al., 2021). To circumvent this difficulty,
123 we develop a parsimony model of the global water cycle involving only the very necessary concepts and
124 constitutive equations, following inspiration from current dynamic vegetation model simplifications
125 using eco-evolutionary optimality concepts (Harrison et al. 2021), or theoretical models catching
126 complex processes into few simplification rules (Dakos et al. 2024).

127 Some examples of parsimony models (also called low-complexity models) demonstrate their
128 power to enlighten our vision of complex systems in all scientific fields. One may cite Lorenz's
129 dynamical model showing the divergence of meteorology governing equations (Lorenz, 1963); Mc
130 Kenzie's model wrapping up in a couple of equations sedimentary basins motion dynamics (Mc Kenzie,
131 1978). The theory of plate tectonics (e.g. Morgan, 1968; Le Pichon, 1968) is probably the best example
132 of assembling unrelated geophysical fields into a coherent, planet scale framework. This integrative
133 process brought into a comprehensive view isolated research fields: mountains building processes,
134 thermal evolution of the lithosphere, divergence of oceanic plate motions and seismology. These
135 examples illustrate how a scientific maze can be sometimes transformed into a solvable puzzle.

136 In the context of our study, a built-in, low-complexity model will aim to provide long time scales
137 simulation by imposing mass conservation along the global water cycle across all components:
138 continental surface and groundwater, vegetation and atmosphere. Although our model will be not able
139 to predict small scale (temporal and spatial) dynamics, it will provide time dependent and asymptotic
140 dynamic of the water cycle. Thanks to its numerical efficiency, this parsimony approach will allow to
141 investigate the sensitivity of model parameter and various model setup changes. To setup a low-
142 complexity model of forest/rainfall interaction, we organize our study as follows: first, we re-examine
143 the data showing the correlation between the large natural forests and annual precipitation on the
144 geographical areas studied by MG2007 with a specific focus on Australia; secondly, we build a
145 simplified numerical model of the water cycle from ocean to continent; thirdly, we present some
146 numerical experiments in order to decipher the parameters controlling regional scale precipitation;
147 finally, we propose an integrated view of forest/water relationships.

148
149 **2.1 Precipitation and forest coverage**
150
151 We present here 10 profiles that have been studied by MG2007 and subsequent papers (Fig. 1a).
152 Two are related to largely forested areas in tropical areas (the Amazon and Congo basins). Five profiles
153 correspond to a partially forested zone: two in temperate zones (from the Appalachians to the inner US
154 Great Plains, and East of the Mississippi basin), and three in boreal areas (the Ob and Yenisey basins,
155 Siberia, and the McKenzie basin, Canada). Finally, the remaining three profiles cross mostly deforested
156 areas (West Africa along longitude 5°E, North-East China and Northern Australia).

157 In order to examine the spatial evolution of the mean precipitation along these transects, from
158 200km seaward towards the inner lands, we used satellite imagery and remote sensing associated to the

159 GIRAFE database (Niedorf et al., 2024). Although coarser than other databases for precipitation,
160 GIRAFE has the advantage of providing data both over continents and oceanic areas at 1° resolution.
161 Here, we computed the mean annual precipitation over the 2010 decade. Since the transects cover a
162 large range of precipitation conditions, for each transect we normalized the mean annual precipitations
163 with their value at the coast (Fig. 1b). Finally, the local forest coverage is estimated from the percent of
164 tree cover supplied by the Global Forest Change database at year 2000 (Hansen et al., 2013).
165
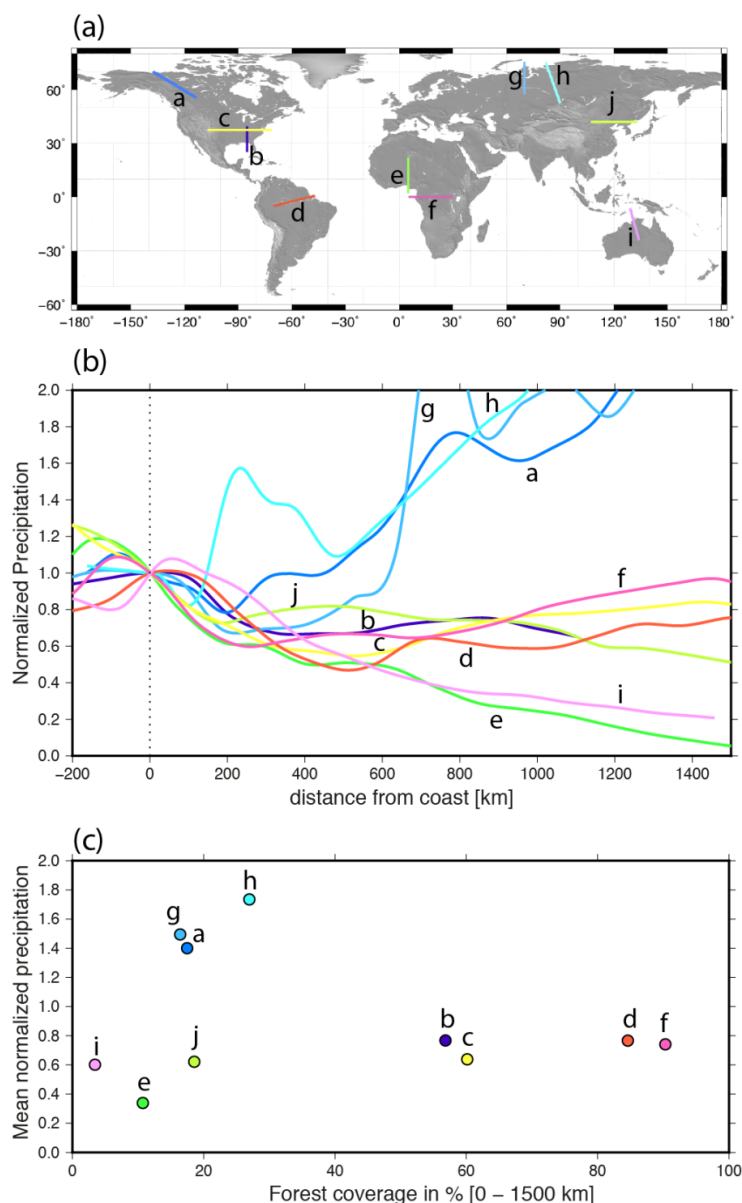
166
167 *Figure 1. MG2007 profiles revisited using mean annual precipitations estimated from the GIRAFE*
168 *database from 2010 to 2020. a) Geographical location of the 10 profiles. From west to east position of*
169 *the oceanic starting point of the transects, the labels correspond to the McKenzie basin (a), East of the*
170 *Mississippi basin at longitude 85°W (b), Eastern North America at latitude 37.5°N (c), the Amazon*

4

171 *basin (d), West Africa at longitude 5°E (e), the Congo basin at latitude 0°N (f), the Ob basin (g), the*
172 *Yenisey basin (h), North Australia (i) and East China at latitude 42°N (j). b) For each transect, the*
173 *mean annual precipitation profile normalized by its value at the coast, as a function of distance to the*
174 *coast. Negative distances correspond to the oceanic domain. Colors and labels on the right side of the*
175 *figure identify the profiles. c) For each profile, we consider the mean annual precipitation over the*
176 *1500 first km on the continent side, normalized by the mean annual precipitation over the 200 first km*
177 *on the oceanic side. These values are plotted as a function of the percentage of tree coverage over the*
178 *first 1500 km determined from the Global Forest Change database.*
179
180 A slight positive trend is observed between forest coverage and precipitation normalized to the
181 ocean and most of these transects reveal that precipitation attenuation from ocean towards inner land is
182 mitigated by the presence of forests. In extreme cases like Amazon or Congo basins, the annual
183 precipitations as far as 1500 km inland are as high as along the coast (Fig. 1b-c). However, the
184 correlation between forest coverage and rainfall is not as clear as claimed by MG2007. This is not
185 surprising as many other factors contribute to pluviometry spatial distribution: atmospheric currents,
186 troposphere temperature, daily and seasonal effects, orographic influences. For example, Ob, Yenisey
187 and McKenzie profiles are clearly influenced by temperature increase from polar zone to cold temperate
188 climate to the south, leading to significant southward increase of precipitation. Considering the
189 numerous potential factors that may interact – even acknowledging a slight positive correlation between
190 forested areas and precipitation (Fig. 1c) – it seems not possible to enlighten a causal relationship
191 between forest and precipitation only on the base of observations.
192 To complement the previous data, we also examine the case of Australia, a continent isolated
193 between Indian and Pacific oceans. Besides the GIRAFE and the Global Forest Change databases
194 mentioned above, we extracted two additional physical values (evapotranspiration and relative
195 humidity) from the JRA-55 climate dataset (Ebita et al., 2011). In the following, these values are
196 averaged over two decades (2002-2021).
197 Australian vegetation is mostly coastal (east and north coast), the remaining part being covered
198 by only sparse vegetation (Fig. 2a). Evapotranspiration distribution (Fig. 2b) is spatially associated with
199 vegetation coverage and is also well correlated with average precipitation pattern (Fig. 3c). This map
200 shows also that oceanic precipitations are intense to the north (monsoon effect) but also that the Pacific
201 Ocean to the east is quite rainy (1000 mm/yr) with respect to Indian Ocean to the west at the same
202 latitude (250 mm/yr). This latter effect might be the combination of several factors: (1) high oceanic
203 humidity to the east, (2) high vegetation evapotranspiration along the eastern coast, (3) humidity
204 advection by trade winds, and (4) atmospheric drying over the Australian central desert. Relative
205 humidity (RH) pattern at ground level displays the same east/west asymmetry (Fig. 2d), also revealing
206 an interesting feature: a systematical RH decreases from ocean to continent all around Australia, with
207 damping distance ranging from almost zero on the west coast to ~600 km on the south east coast.
208
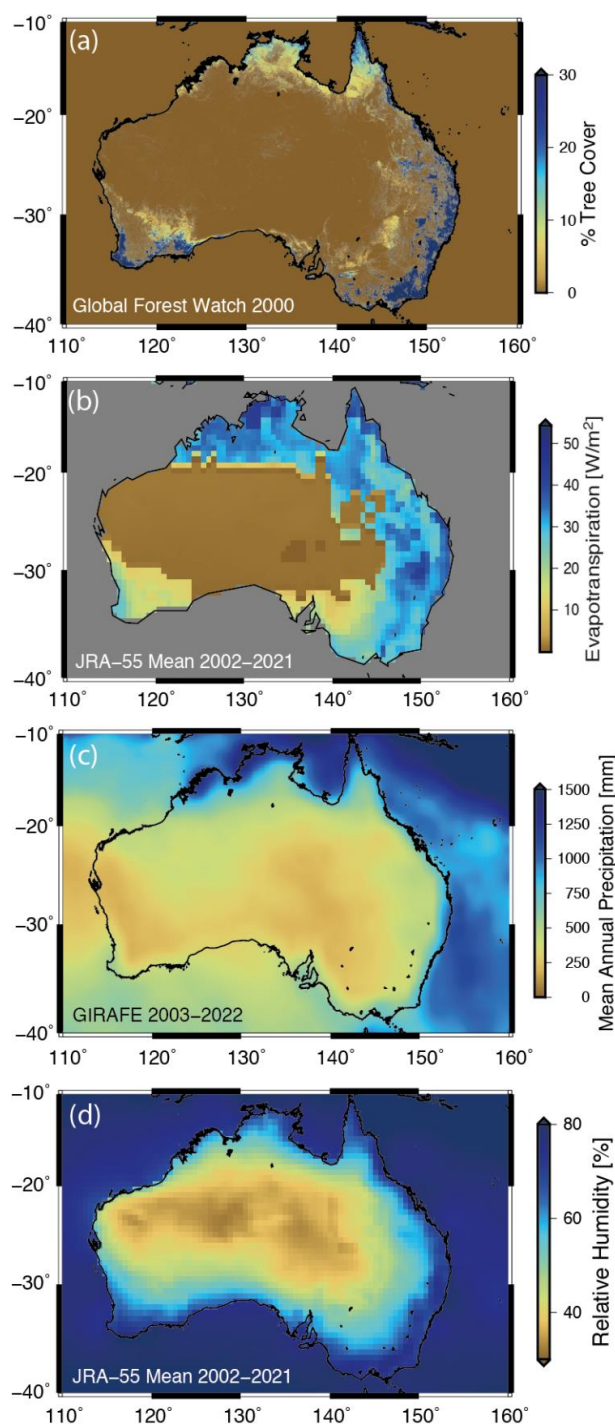
210 *Figure 2. Averages atmospheric and vegetation distribution on Australia (a) Tree cover percent in*
211 *2000 (Global Forest Change) (b) Averaged evapotranspiration 2002-2021 (JRA-55) (c) Averaged*
212 *precipitation 2003-2022(GIRAFE) (d) Average Relative humidity at 1000hPa 2002-2021(JRA-55)*

213
214   These atmospheric patterns suggest that oceanic moisture, its transport over the continent and
215 vegetation evapotranspiration combine in a complex way to provide precipitation pattern. This remark
216 is aligned with numerous research papers studying these processes interactions (e.g. Eltahir, 1998). At
217 this point, it should be reminded that the description above embraces only aerial water flow processes,
218 while underground water storage is of prime importance for feeding vegetation with water. Face to the
219 need to close water budget cycling back and forth between ocean and continent, we present an integrated
220 model approach of atmospheric and hydrologic water transport.
221
222 **3. Parsimony water cycle model**
223
224   Computing aerial and underground water transport involves three conservation equations for the
225 mass, momentum (or forces) and energy. As we are chiefly interested by water mass budget and long-
226 term climatic processes, we use mass conservation as a pivotal way to evaluate water motion during the
227 water cycle (Fig. 3). Momentum and energy equation are not solved, implying that variables like wind
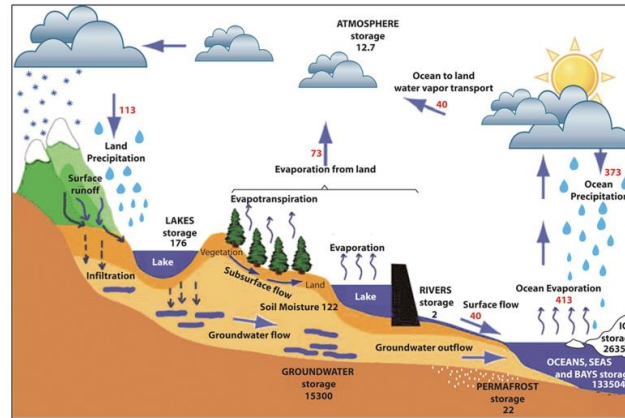228 velocity and temperature are directly included as input functions into water transport equations.
229

230
231   *Figure 3. hydrological cycle (from Gimeno et al., 2012).* Black numbers give estimates of the
232 observed main water reservoirs in 10^3 km^3 and red numbers indicate the flow of moisture through the
233 system in 10^3 km^3 yr^{-1}.
234
235 3.1 Tropospheric water vapor transport:
236
237   All flowing continental waters ultimately come from ocean evaporation carried by the
238 atmosphere. We assume that horizontal water transport mostly occurs as vapor into the lower
239 troposphere represented by a single layer having a thickness of about 5 km. We consider a 2D vertical
240 cross-section (Fig. 4), for which all physical variables represent average troposphere behavior, and the
241 tropospheric water vapor (WV) at a given point is governed by the following mass conservation
242 equation:
243
244     $\frac{\partial C}{\partial t} = div[-D_h grad_x(C) + vC] + \frac{\rho_w g}{P_{atm}}(\dot{E} - \dot{P})$ (eq. 1)

245   where C is water vapor concentration, D_h is horizontal dispersion, v is wind velocity, ρ_w is water
246 density, g is gravity acceleration, P_{atm} is surface atmospheric pressure, $\dot{E}$ is evaporation/
247 evapotranspiration rate and $\dot{P}$ is precipitation rate (Table 1 provides units).Therefore, WV horizontal
248 transport is controlled by both concentration gradient and wind advection (see Rasmusson, 1968) for a

249 similar formulation). This equation converts a vertically integrated balance of WV into its concentration
250 (Gimeno et al. 2012, eq. 7). We also include a dispersion term that is generally not implemented in
251 simplified circulation models. Indeed, we conjecture that horizontal dispersion is of particular interest
252 for large scale WV distribution, as concentration gradients continuously sustain WV flow from wet to
253 dry areas. Apart from WV dispersion, effective horizontal dispersion can be estimated by combining
254 observation and modelling of long-range atmospheric transport of various products: nuclear products
255 dispersion (Ishikawa, 1995), volcanoes gas emission (Tiesi et al. 2006), pollutant plume transport (Pisso
256 et al. 2009), providing dispersion values ranging between 10^3 and 10^5 m^2/s. We also consider water
257 sources and losses: evaporation (ocean) and evapotranspiration (plants) provide source terms $\dot{E}$ of eq.
258 1, while rain rate is associated to water loss $(-\dot{P})$. The sum of all terms of the right-hand side of eq. 1
259 corresponds to WV concentration rate change at a given location.
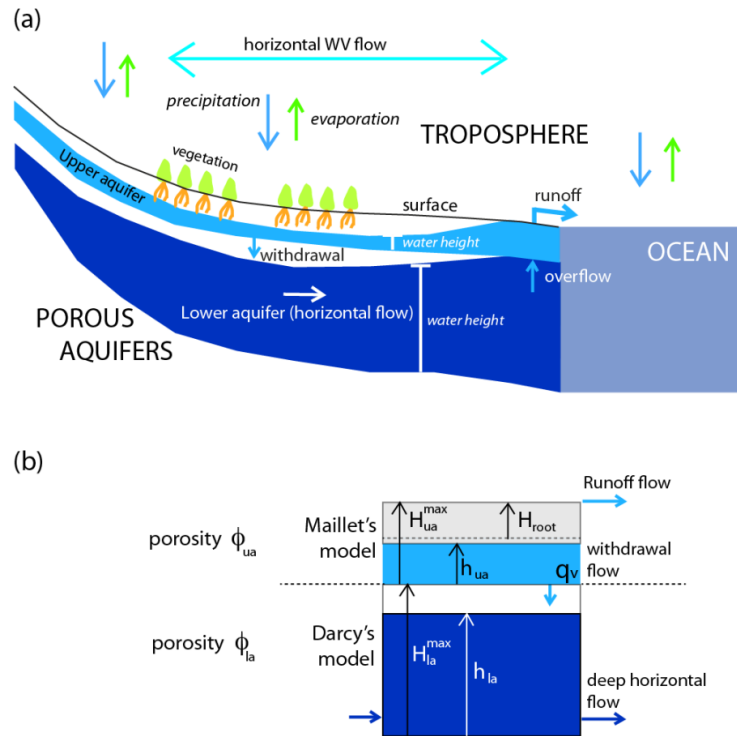
260

261 *Figure 4. a) simplified water transfer model including troposphere / vegetation / hydrosphere*
262 *interactions ; b) equivalent model using notations used throughout the text and eqs. 7 and 8. Case*
263 *associated to eqs. 7a and 8a is represented.*
264

265   Maximum WV concentration in the atmosphere is controlled by the Clausius-Clapeyron (C-C)
266 relation integrated over the whole tropospheric column, thus providing the upper estimate of precipitable
267 water vapor (PWV$_{C-C}$). We adapt here the formulation of Reitan (1963):
268

269 $PWV_{C-C} = 0.01 \cdot exp\,[0.1102 + 0.06138T]$ (eq. 2)
270

271 where T is ground temperature in °C (Fig. 5). For sake of simplicity, we do not consider here the
272 variation of ground temperature as a function of altitude, meaning that temperature in eq. 2 is
273 independent on ground elevation. The maximum water vapor concentration C_{C-C} can be expressed as:
274

275    $C_{C-C} = \frac{\rho_w g}{P_{atm}} PWV_{C-C}$ (eq. 3)
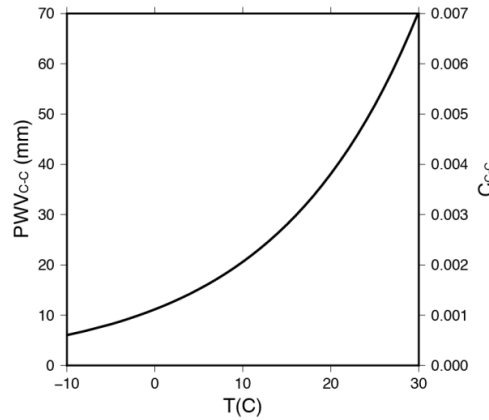
276

277
278
279   *Figure 5. Maximum precipitable water vapor (PWV$_{C-C}$) and concentration (C$_{C-C}$) associated to the*
280   *Clausius-Clapeyron law (from Reitan, 1963)*
281

282   The precipitation rate largely depends on the relative humidity of the atmosphere RH defined as
283    $100(C/C_{C-C})$. Also, it has been noticed that the probability of precipitation below a given saturation
284   threshold is very low, while it is rapidly and non-linearly increasing around this threshold (Neelin et al.,
285   2009). We mimic this behavior using a power law formulation controlled by its exponent n (ref?) to
286   explicitly define the precipitation rate (eq. 4). In addition, geochemistry studies provide some values of
287   water droplet residence time in the atmosphere ranging between 2 and 10 days (Läderach and Sodemann,
288   2016; Gimeno et al., 2012). Therefore, we choose a simplified relationship where the rain rate is
289   controlled by a characteristic time t_{rain}. Despite the relationship between extreme precipitations and
290   C-C is not always linear for temperature higher than 15°C (Drobinski et al., 2016), we make the
291   simplified hypothesis that rain rate $\dot{P}$ scales with the maximum amount of tropospheric water PWV_{C-C},
292   leading to the following constitutive relation (see also Figure 6):
293

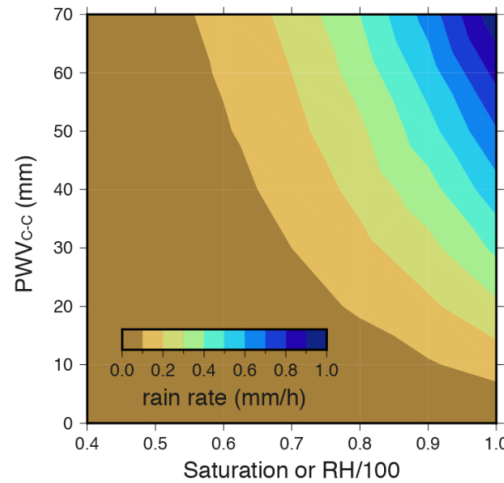294 $\dot{P} = \frac{PWV_{C-C}}{t_{rain}} \left(\frac{RH}{100}\right)^n$ (eq. 4)

296 *Figure 6. Rain rate associated to eq. 4 and Table 1*
297
298
299   3.2 Evaporation and evapotranspiration
300
301   Due to the complexity of evaporation processes acting over water bodies (lakes and ocean),
302   experimental and theoretical studies do not converge onto a unique formula for the evaporation rate $\dot{E}$.
303   Fortunately, only few atmospheric parameters control evaporation: wind, relative humidity of the lower
304   atmosphere (RH), surface temperature and solar radiation (Filimonova and Trubetskova, 2005; Singh
305   et al., 1995). On land, since plant evapotranspiration results from complex physical and biological
306   mechanisms, potential evapotranspiration ET_0 appears to be the most common concept defined as the
307   theoretical rate of plant (shallow rooted grassland) transpiration when soil water content is not limiting
308   and ensures optimal stomatal conductance, associated to the Penman-Monteith formulation (Penman,
309   1948; Monteith, 1965). However, this formula is not easy to use for data assimilation and efforts were
310   made to associate ET_0 with atmospheric observations as for the oceanic case, that is relative humidity,
311   surface temperature, and solar radiation. Because water bodies and vegetation share common controlling
312   parameters, we find convenient to use the polynomial formula of Alexandris and Kerkides, (2003) to
313   model within a single equation both oceanic evaporation and empirical plant transpiration:
314
315     $ET_0 = f[S_{irr}, T, RH]$ (eq. 5)
316
317   where S_{irr} represents solar irradiance and f a polynomial function of degree 2 in S_irr, T and RH. From
318   an integrative model viewpoint, this assumption presents the interest to embed into a single
319   parametrization vegetation evapotranspiration and water bodies evaporation (Fig. 7). On land, we
320   introduce a scaling coefficient F_c representing the impact of leaf area on kilometer scale transpiration.
321   We therefore mimic a desert using $F_c = 0$ (assuming that no evaporation takes place) and a full forest
322   coverage using $F_c = 1$. The effective potential evapotranspiration formula is given by:
323
324     $ET_p = F_c \cdot ET_0$ (eq. 6)
325

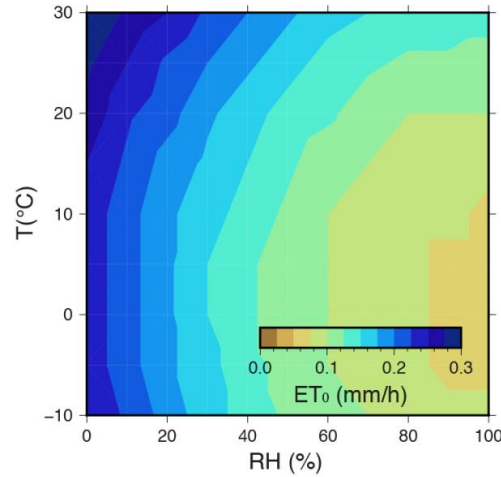327 *Figure 7. ET₀ as a function of relative humidity RH and temperature T (from* Alexandris and Kerkides,
328   2003).
329

330   Even if potential evapotranspiration may reach several mm per day, real plant evapotranspiration
331 rate ultimately depends on the soil water amount that roots are able to extract. We consider a model of
332 trees equipped with roots reaching a depth H_{root}, assuming trees living over a shallow aquifer of
333 thickness H_{ua} in which the water height h_{ua} dynamically evolves between 0 and H_{ua} due to root uptake
334 and underground water motion (see Fig. 4b). Therefore, real evapotranspiration rate $\dot{E}$ takes two
335 admissible values:
336
337 $h_{ua} \leq H_{ua} - H_{root} \quad then\ \dot{E} = 0$ (eq. 7a)
338 $h_{ua} > H_{ua} - H_{root} \quad then\ \dot{E} = ET_p$ (eq. 7b)
339
340 3.3 Runoff and underground water flow
341
342   Rainwater reaching the soil surface follows one of the three paths: (1) shallow infiltration, root
343 uptake and evapotranspiration, (2) deep infiltration, or (3) surface runoff by direct river connection or
344 by upper aquifer overflow. We implement upper aquifer overflows using the following conditions for
345 the model, insuring that $h_{ua} = H_{ua}$ in eq. 8b so that runoff $\dot{R}$ takes place:
346
347 $h_{ua} \leq H_{ua} \ then \quad \dot{R} = 0$ (eq. 8a)
348 $h_{ua} > H_{ua} \ then \quad \dot{R} = d\ h_{ua}/dt$ (eq. 8b)
349
350   Modeling groundwater transfer is a vast research field implying a variety of flow processes and
351 water/rock interactions (Ntona et al., 2022). One difficulty of setting a continent-scale hydrogeological
352 model is the high heterogeneity of underground water aquifers due to interplay between geological
353 processes, relief, topography and surface rivers, thus resulting in a great diversity of groundwater
354 residence times, concepts and models. As for the troposphere, we assume that water mass conservation
355 is achieved and we simply distinguish two gravity-controlled water flow processes. The upper aquifer
356 is treated like a partially saturated zone formed by the soil and subsurface rocks. A useful soil-water
357 interaction is provided by the Richards equation (Van Dam and Feddes, 2000). However, this model
358 incorporates many soil parameters that renders it too complex for our purpose. We adopt a simpler model
359 derived from Maillet's reservoir model (Maillet, 1905; Fleury et al., 2007). This reservoir has a thickness
360 H_{ua} already defined, and its withdrawal flow q_v at a given horizontal location is provided by the upper
361 aquifer storage $\phi_{ua} h_{ua}$ (ϕ_{ua} being the porosity of the medium) divided by the characteristic time t_{ua} of
362 the Maillet's reservoir:
363

364 $q_v = \frac{\phi_{ua} h_{ua}}{t_{ua}}$ (eq. 9)

365
366 The lower aquifer receives water from above and insure near horizontal flow according to hydraulic
367 head gradient. We use the original Darcy's formulation (Hubbert, 1956) stating that horizontal flow is
368 occurring as the product of the hydraulic conductivity K and the hydraulic head gradient of the lower
369 reservoir free surface. Estimate of average hydraulic conductivities for large scale aquifers is dependent
370 on many geological and mechanical parameters. Such an integrated parameter is provided at basin-scale
371 using geostatistic methods (e.g. El Idrysy and De Smedt, 2007) and we adopt conductivity values
372 ranging from 10^{-3} to 10^{-1} m/s. The aquifer hydraulic head involves the topographic elevation z and the
373 lower aquifer dynamic height h_{la} that are both depending on horizontal x-coordinate. The underground
374 water advection is controlled by the following conservation equation:

375
376 $\frac{\partial h_{la}}{\partial t} = div\left[-Kgrad_x(z + h_{la})\right] + q_v$ (eq. 10)

377
378 Where the upper aquifer withdrawal flow is the source term of the lower aquifer (note the similarity
379 between eqs. 10 and 1). Water overflows into the upper reservoir if the following condition is met:

380
381 $h_{la} \geq H_{la}$ (eq. 11)

382
383 meaning that q_v becomes negative in order to insure the compatibility equation $h_{la} = H_{la}$. For such a
384 case, upper aquifer fills from below according to the situation pictured in Fig. 4a (near the coast).

385
386
387
388 3.4 Numerical formulation

389
390 Despite our goal to provide a parsimony formulation of the global water cycle, we are left with a fairly
391 complex dynamical system including 3 variables (C, h_{ua} and h_{la}), 11 equations (1-11) and more than
392 thirty model parameters (Table 1). We therefore implement a dedicated numerical treatment combining
393 finite elements for horizontal water transfer into the troposphere and the lower aquifer, coupled to a
394 finite difference scheme for vertical transfer (evaporation and vertical infiltration) in the upper reservoir.
395 A FORTRAN 95 code was specifically developed to compute dynamic water exchanges between ocean,
396 troposphere and hydrosphere. We perform different tests to insure solution stability with respect to time
397 and space discretization, also checking mass conservation over time.
398 Each experiment corresponds to 40 elements (100km per element) in order to capture solutions
399 spatial variations, using a 1-hour time step to ensure stability of the finite difference scheme. The
400 physical duration of each experiment is set to 300 years in order to reach stationary solution for all
401 presented cases. The computation is achieved after 17s using a 3.4 GHz Intel Core i5 processor (2013).

402
403
404

405

406
407 TABLE 1
408 MODEL PARAMETERS AND VALUES. Model's variables are given in bold, parameters variations appear in red.

Symbol	Unit	Used values	Description
GEOMETRY			
x	m		Horizontal coordinate
z	m		Topographic elevation
z_{max}	m	[100; 1000]	Maximum topographic elevation
L_o	km	2000	Ocean length
L_c	km	2000	Continent length
TROPOSPHERE			
$\mathbf{C}$	**kg/kg**		**Water vapor concentration**
C_{C-C}	kg/kg		Maximum water vapor concentration
S_{irr}	W/m^2		Solar irradiance
P_{atm}	Pa	10^5	Ground atmospheric pressure
T_{ocea}	°C	20	Oceanic air temperature
T_{cont}	°C	[17; 20; 23]	Continental surface temperature
PWV	m		Precipitable water vapor
PWV_{C-C}	m		Maximum precipitable water vapor
$\dot{P}$	m/s		Precipitation rate
P_c	m		Cumulated precipitation
ρ_w	kg/m^3	10^3	Water density
D_h	m²/s	[10^3; 10^4; 10^5]	Horizontal dispersion
v	m/s	[−1; 0; +1]	Wind velocity
d_c	-	0.5	Cloud spatial density
n	-	4	Saturation exponent
t_{rain}	days	3	Rain critical time
VEGETATION			
F_c	-	[0; 0.1; 1]	Forest coverage ratio
ET_0	mm/day		Reference evapotranspiration rate
ET_p	mm/day		Potential evapotranspiration rate
H_{root}	m	5	Rooting depth
$\dot{E}$	m/s		Real evaporation rate
E_c	m		Cumulated evaporation
AQUIFERS			
$\mathbf{h_{ua}}$	**m**		**Upper aquifer water height**
H_{ua}^{max}	m	10	Upper aquifer thickness
ϕ_{ua}	-	0.1	Upper aquifer porosity
S_{ua}	m		Upper aquifer storage ($\phi_{ua} h_{ua}$)
t_{ua}	days	[10^1; 10^2; 10^3]	Upper aquifer withdrawal time
q_v	m/s		Upper aquifer withdrawal rate
$\mathbf{h_{la}}$	**m**		**Lower aquifer water height**
H_{la}^{max}	m	100	Lower aquifer thickness
ϕ_{la}	-	0.02	Lower aquifer porosity
S_{la}	m		Lower aquifer storage ($\phi_{la} h_{la}$)
K	m/s	[10^{-3}; 10^{-2}; 10^{-1}]	Lower aquifer hydraulic conductivity
$\dot{R}$	m/s		Runoff rate
R_c	m		Cumulated runoff
S_{rel}	%		Overall aquifers relative storage

409
410

411

13

412 **4. Results of numerical experiments**
413
414 4.1 Geometry, boundary conditions, external forcing and initial state
415
416   We aim to understand the physical factors controlling average continental precipitation P_c at a
417 large spatial scale. We therefore design a 2000 km length continent surrounded by two oceans of
418 equivalent sizes (Fig. 8), assuming the following conditions:
419   - A constant temperature of 20°C is used with tuning solar irradiance for obtaining an oceanic
420   annual precipitation of about 1m (average precipitation rate of 0.12mm/h). We therefore do not
421   account for diurnal and seasonal dynamics.
422   - Initial conditions correspond to (1) a dry troposphere (C = 0 in eq. 1) and (2) dry continental
423   aquifers (h_{ua} = 0 and h_{la} = 0). Continental evapotranspiration therefore equals zero at the
424   beginning of each experiment, meaning that water transport from the ocean via the troposphere
425   is the sole way to fill upper and lower aquifers;
426   - Wind velocity can be set to zero to study the dispersion effect of the troposphere.
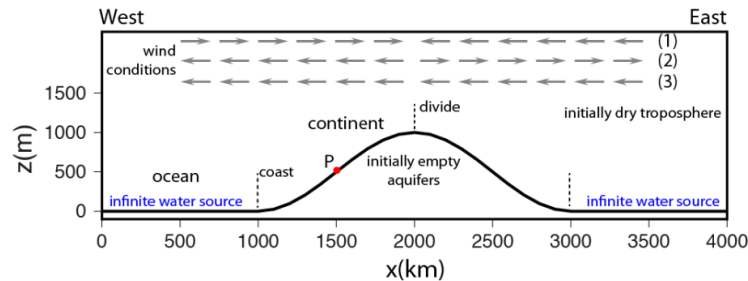427

428
429 *Figure 8. topography and initial conditions for troposphere and continental aquifers. Solid line figures*
430 *topography elevation, while grey arrows represent wind conditions used in 4.4 section: (1) convergent*
431 *system (upwind) from ocean to continent; (2) divergent system (downwind) from continent to ocean,*
432 *and (3) through wind from east to west. Red dot (P) refers to the time evolution of Fig. 12.*
433
434 4.2 Parametric study: vegetation and hydrology
435
436   In a first set of 18 experiments, we assume a tropospheric horizontal dispersion of 10^4 m/s^2 (Table
437 1, see also Pisso et al., 2009). Two values of 0.1 and 1 are assumed for forest coverage ratio in order to
438 mimic respectively sparse and dense forest coverage. We tune upper aquifer withdrawal times over 3
439 orders of magnitude from 10 days (permeable aquifer) to 10^3 days (2.7 years, almost impervious
440 medium). We also test the effect of deep aquifer conductivity variations (10^{-3} - 10^{-1} m/s).
441   All experiments display a quasi-invariance of oceanic precipitation despite the variation of
442 continental parameters over 3 orders of magnitude, indicating that continental parameters have a
443 marginal impact on open sea evaporation controlled by vertical transfer between rain rate (eq. 4) and
444 evaporation (eq. 5). We therefore present annual averaged continental precipitation and
445 evapotranspiration normalized by oceanic precipitation (P_{norm} and E_{norm} on Fig. 9).
446   Sparse forest experiments (F_c=0.1) display a modest normalized precipitation on continents never
447 exceeding 20% of the oceanic value over the whole aquifer parameters range (Fig. 9a). By contrast,
448 dense forest experiments (F_c=1) reveal a larger precipitation, increasing from 15% (high aquifer
449 conductivity) to 90% (low aquifer conductivity) as shown by Fig. 9b. Evapotranspiration variations are
450 closely associated with precipitation trends for both sparse and dense experiments (Fig. 9c,d) suggesting
451 a causal link between these two quantities.
452   Considering aquifer's storage (defined as % of the full capacity $S_{ua} + S_{la}$), smaller differences
453 are observed between sparse and dense cases (Fig. 9e, f). Rather, deep aquifer conductivity appears like
454 the main controlling factor with lower values leading to higher water storage. Upper aquifer withdrawal
455 times also display significant impact on water heights, smaller values favoring lower aquifer filling. It

456   emerges that dense forest water storage is higher than its sparse counterpart for high conductivity and
457   high withdrawal time, while this storage becomes smaller than sparse water storage for low conductivity
458   and low withdrawal time. Therefore, water storage appears to be balanced by the whole water cycle
459   dynamics, including evapotranspiration, aquifer's parameters, and precipitation.
460
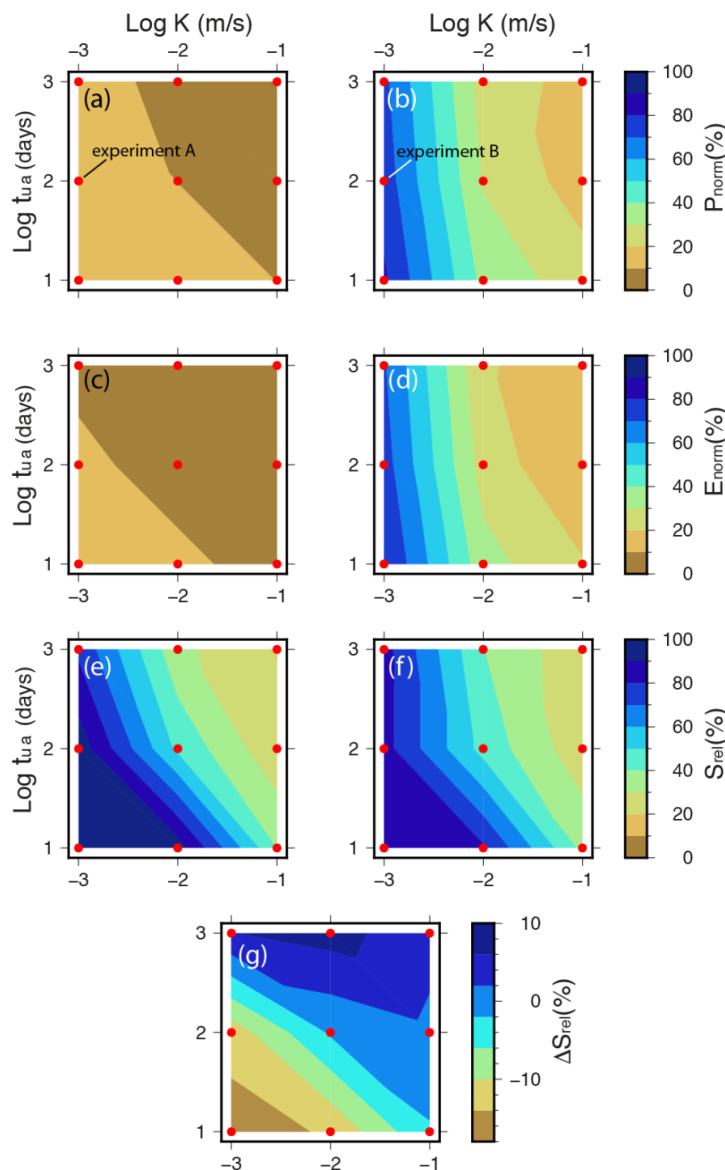
461
462   *Figure 9. Annual continental precipitation relative to its oceanic value as function of lower aquifer*
463   *hydraulic conductivity and upper aquifer withdrawal time after 300yrs; each circle represents an*
464   *experiment while colored maps result from linear interpolation; (a, b) annual precipitation*
465   *normalized by oceanic precipitation for respectively sparse and dense forests in %; (c, d) annual*
466   *evapotranspiration normalized by oceanic precipitation for respectively sparse and dense forests in*
467   *%; (e, f) overall aquifer storage in % of its full capacity for respectively sparse and dense forests; (g)*
468   *dense forest storage minus sparse forest storage in %.*

469
470   4.3 Sparse and dense forests experiments

471   To understand the causal link between model's parameters and dynamical outputs such as
472   evaporation, precipitation and aquifer storage, we track temporal and spatial evolution of some of the
473   proposed experiments. We present two solutions corresponding to a withdrawal times of 100 days
474   (permeable aquifer) and an aquifer conductivity of 10^{-3} m/s (named experiments A and B on Fig. 9a and
475   Fig. 9b, respectively). For a sparse forest, the solution displays a pronounced WV concentration gradient
476   near the coastline, leading to a constant WV concentration for times larger than 200 yrs (steady state
477   solution, see Fig. 10a). Evapotranspiration and precipitation reach the same constant value ($\dot{E} = \dot{P}$) on
478   the continent (Fig. 10b), revealing the lack of horizontal WV flow. Near the coastline, aquifers overflow
479   and produce some local rivers while water transport occurs underground inland (Fig. 10c). Due to low
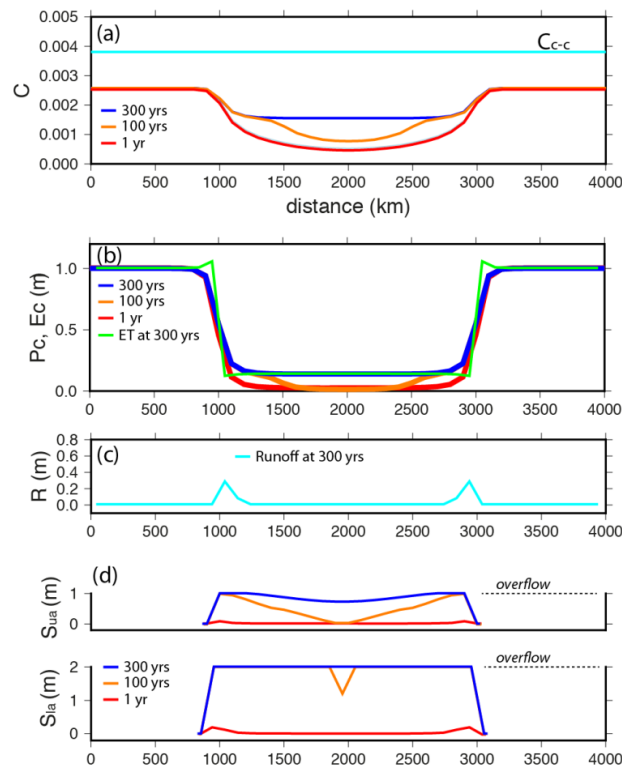480   aquifer conductivity, aquifers are 90% full throughout the continent (Fig. 10d) as also displayed on Fig.
481   9e.
482
483
484

485
486
487   *Figure 10. Steady state solutions (sparse vegetation, experiment A) (a) troposphere WV concentration*
488   *(red-orange-blues lines) and C-C concentration yield (cyan line); (b) cumulated precipitation (red-*
489   *orange-blues lines) and evaporation (green); (c) runoff (cyan); (d) upper and lower aquifer storage.*
490
491   Dense forest solution reveals a different evolution with a progressive WV concentration increase
492   during 300 years until it reaches a much higher value than sparse value experiment (Fig. 11a).
493   Evapotranspiration and precipitation also become equal for times larger than 200 years (Fig. 11b). Due
494   to active upper aquifer pumping by the trees, no runoff takes place (Fig. 11c) as the upper aquifer is

495 filled at only 50% of its maximum capacity (Fig. 11d). As a result, dense forest overall aquifers are only
496 partially filled and depleted by 15% with respect to sparse forest (Fig. 9g).
497
498
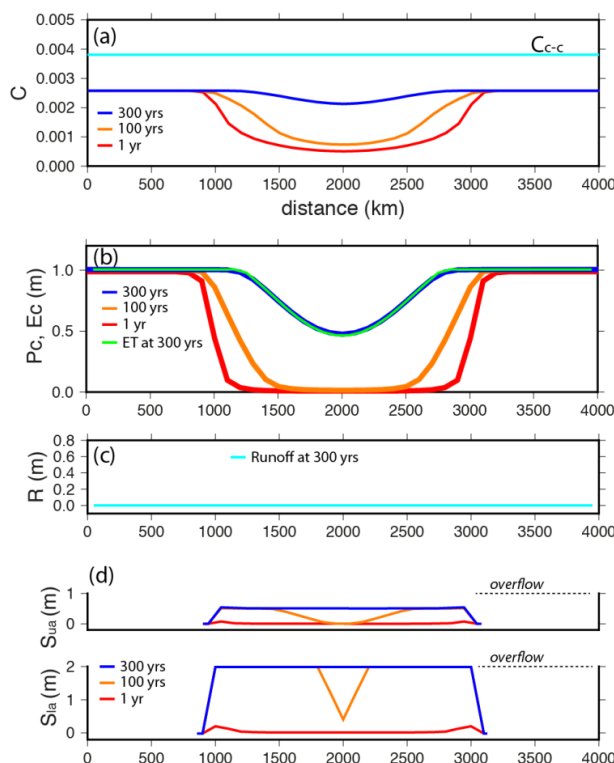
499
500
501 *Figure 11. Steady state solutions (dense vegetation, experiment B) (a) troposphere WV concentration*
502 *and C-C concentration yield (cyan line); (b) cumulated precipitation and evaporation; (c) runoff; (d)*
503 *upper and lower aquifer storage.*
504

505   In order to identify functional interplays between atmospheric, biophysical and hydrological
506 solutions, we track time evolution of dense forest experiment (B) at a point P located 500 km from the
507 coast (x=1500 km, Fig. 8 and 11). A staggered evolution takes place from empty reservoirs to steady-
508 state values following atmospheric and hydrologic steps:
509   (1) initial WV concentration (set to 0) rapidly increases within 1 year, resulting into a step in Fig.
510   12a due to horizontal WV dispersion from ocean to continent;
511   (2) progressive deep aquifer filling from 0 to 40 years;
512   (3) then, deep aquifer overflows into the shallow aquifer that progressively fills from 40 to 130
513   years;
514   (4) upper aquifer head reaches root depth at 130 years thus allowing evapotranspiration increase
515   until its stabilized value at 145 years. Due to EVT increase, WV concentration positively
516   jumps, thus triggering precipitation by a factor of 7.5 (from 0.1m/yr at 130 years to 0.75 m/yr
517   at 145 years).

518
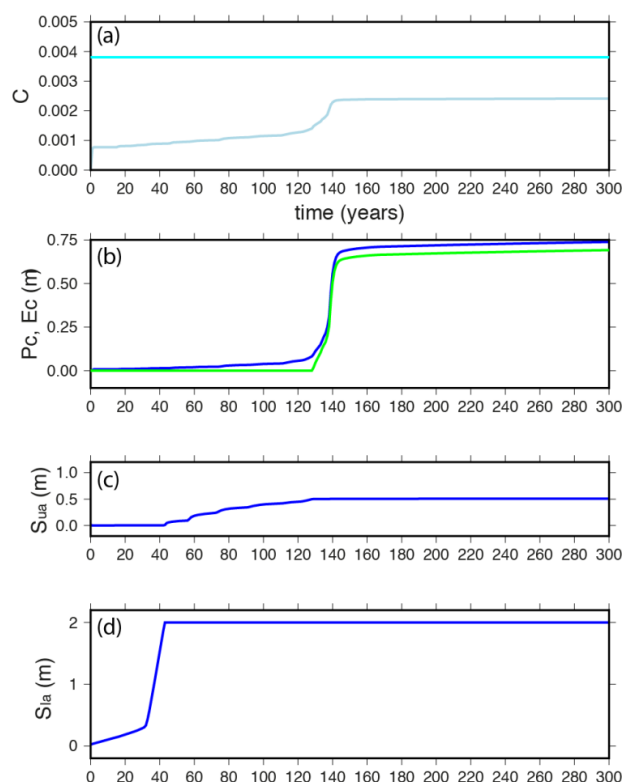
Figure 12. Time evolution at 500km from coast (dense vegetation, experiment B) (a) troposphere WV concentration and C-C concentration yield (cyan line); (b) cumulated precipitation (blue line) and evaporation (green line); (c) upper aquifer storage; (d) lower aquifer storage.

519
520
521
522
523   This retroaction chain involving atmospheric, biophysical and hydrological components
524 systematically occurs in all our models with dense forest parameters, the final consequence being an
525 increase of continental precipitation up to a stabilized value (Fig. 9 and 12). The magnitude of the
526 precipitation increase depends on the capacity of the vegetation to deliver WV to the atmosphere.
527 However, complexity emerges due to the coupling between evapotranspiration capacity and the other
528 elements of the water cycle and especially the groundwater deep aquifer. We therefore explore how
529 tropospheric, topographic, geological and biophysical parameters influence steady state continental
530 precipitations, using the same range of vegetation coverage (0.1 and 1) and lower aquifer conductivity
531 (10^{-3} - 10^{-1} m/s) as for the preceding experiments.

532
533   4.4 Tropospheric parameters: dispersion, temperature and wind

534
535   Because long range chemical dispersion D_h is expected to largely vary with atmospheric
536 conditions, we explore the influence of respectively low (10^3 m/s^2) and high dispersion values (10^5 m/s^2)
537 on normalized precipitation with respect to our reference value of 10^4 m/s^2 (corresponding to red curves
538 on Fig. 13). Sparse vegetation cases reveal a significant precipitation increase (20-100%) for high
539 dispersion values (Fig. 13a) and no change for low dispersion. Dense vegetation experiments magnify
540 this trend with a 30-120% precipitation increase for high dispersion values (Fig. 13b). Noticeably, the
541 largest precipitation variation occurs for low hydraulic conductivity (10^{-3} m/s), while variations remain
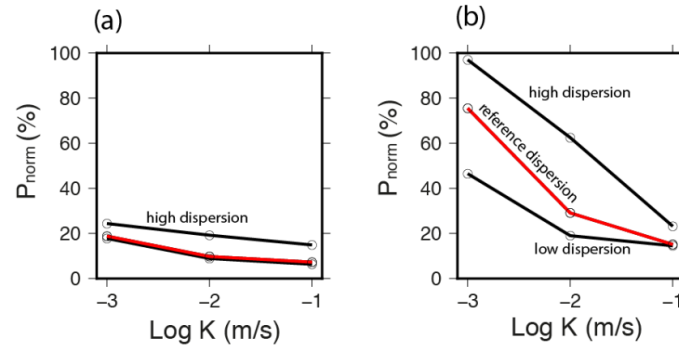542 modest for high hydraulic conductivity (10^{-1} m/s).

Figure 13. Normalized precipitation as a function of tropospheric dispersion (low=10^3 m^2/s; high=10^5 m^2/s, black lines; reference=10^4 m^2/s, red lines) for different hydraulic conductivities (a) sparse vegetation (b) dense vegetation.

We then vary continental temperature with respect to the reference value of 20°C with a -3°C decrease and +3°C increase, the oceanic temperature remaining at 20°C. The impact of those changes is negligible for sparse vegetation cases (Fig. 14a). It appears that the largest changes occur for dense vegetation coupled to low hydraulic conductivity (Fig. 14b). Lower temperature increases precipitation (because the maximum precipitable water vapor PWV_{C-C} limit decreases, see Fig. 5). Higher temperature shows the opposite effect and the precipitation drops from 78 % to 58 %.
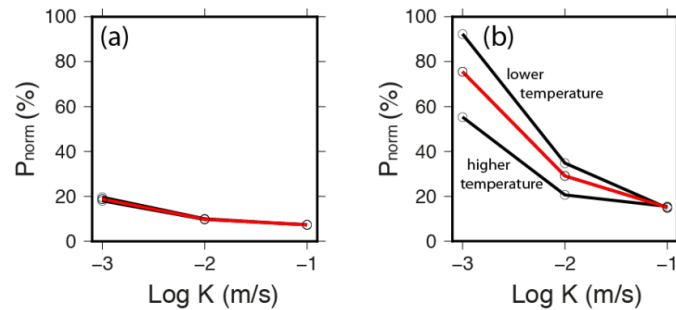

Figure 14. Normalized precipitation as a function of continental temperature (lower=17°C; higher=23°C) for different hydraulic conductivities (a) sparse vegetation (b) dense vegetation.

All previous experiments stand for no advection in eq. 1 (wind velocity v set to zero). We test here three wind conditions: (1) a fully convergent system (upwind) of 1 m/s from ocean to continent, (2) a fully divergent system (downwind) of 1 m/s from continent to ocean, and (3) a through wind of 1 m/s combining upwind on the right (east) side of the model and downwind on the left (west) side of the model (see also Fig. 8 for wind conventions). Imposing a wind condition dramatically changes precipitation patterns for both sparse (Fig. 15a) and dense (Fig. 15b) cases. Downwind condition leads in any case to zero precipitation, suggesting that some continental regions may become completely dry if this wind regime is permanent. At the opposite, upwind cases maximize precipitation by a ratio, relatively to the zero-wind cases, ranging from 2.2 to 7. Interestingly, dense forest cases reveal that continental precipitation may exceed the oceanic value due to a positive combination of dispersion, advection and evapotranspiration bringing moisture to the continent.
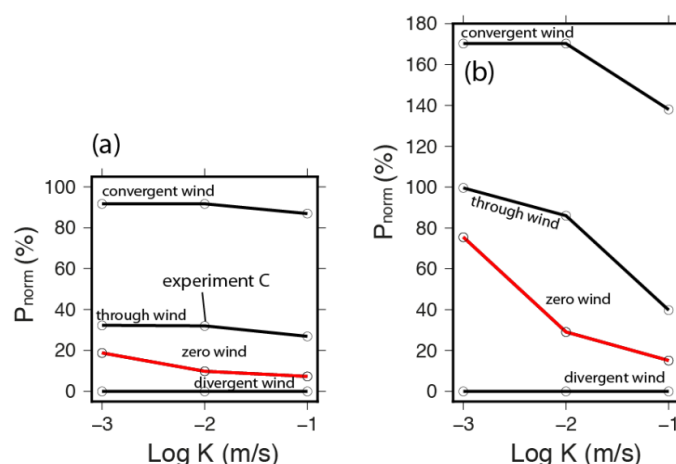
572
573 *Figure 15. Normalized precipitation as a function of wind condition as described in the main text (a)*
574 *sparse vegetation (b) dense vegetation.*
575

576 Through wind condition is insightful as it represents upwind/downwind combination often occurring on
577 Earth with trade winds (tropical zone) and westerlies (tempered zone). Although such experiments
578 present a zero net wind budget for the continent (null divergence in eq. 1), large precipitation increases
579 (50% - 150%) are observed for both sparse and dense vegetation cases with respect to zero wind cases.
580 To highlight this point, we present in Fig. 16 through wind spatial patterns for sparse vegetation case.
581 Upcoming wind from the east leads to asymmetrical WV concentration (Fig. 16a) with higher
582 concentration upwind. Accordingly, precipitation is higher on east coast (Fig. 16b) while west coast
583 remains extremely dry including its oceanic part. Due to low evapotranspiration and low aquifer
584 hydraulic conductivity, aquifers are almost full across the whole continent (Fig. 16c) while runoff mainly
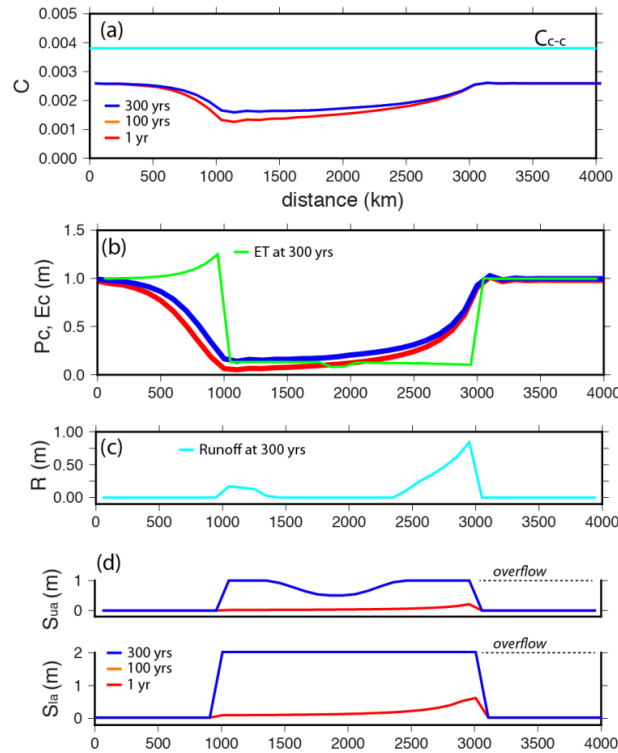585 takes place close to upwind coast to the east (Fig. 16d).
586

587
588 *Figure 16. Steady state solutions (sparse vegetation, through wind condition, experiment C on Fig.*
589 *15a (a) troposphere WV concentration; (b) cumulated precipitation and evaporation; (c) runoff; (d)*
590 *upper and lower aquifer storage.*
591
592 4.5 Topographic parameters
593
594 Topography influences both orographic conditions (modeled here through temperature and
595 integrated WV) and hydrological flow. We recall that surface temperature in eq. 2 (Reitan formula) is
596 independent on ground elevation. Therefore, topography only modifies hydrological flow and the
597 orographic effect on precipitation is not accounted. We check hydrological influence by introducing a
598 low topography with a maximum elevation of 100 m, 10 times smaller than for the previous models. In
599 this way, we modify the contribution of the hydraulic head of underground water motion (eq. 10). While
600 this parameter change has a relatively minor influence for sparse vegetation cases (Fig. 17a),
601 precipitation increases up to 150% for dense vegetation cases depending on lower aquifer conductivity
602 values (Fig. 17b). This water cycle enhancement is due to a global interplay between horizontal water
603 flow lowering, reservoir filling and the increase of evapotranspiration as already detailed above (see Fig.
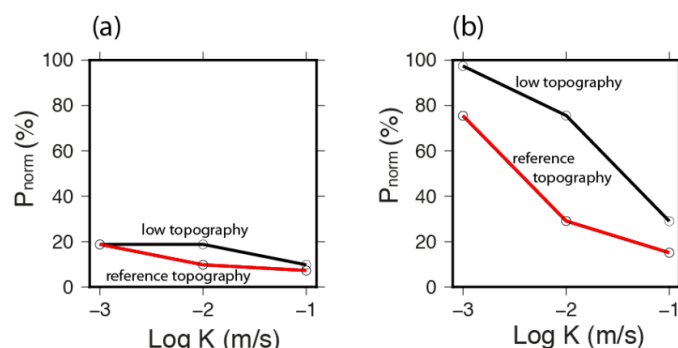604 12).

21

605
606   *Figure 17. Normalized precipitation as a function of topography condition (red line=reference, black*
607   *line=low topography) (a) sparse vegetation (b) dense vegetation.*
608
609   <u>4.6 Forest geographic location</u>
610
611   Until now we have considered a homogeneous vegetation density with sparse ($F_c = 0.1$) and
612   dense cases ($F_c = 1$) cases. We now consider a 400 km-long densely forested area ($F_c = 1$) at a distance
613   to the coast varying from 0 km (coastal forest) to 800 km (central forest), the rest of the continent being
614   fully deforested ($F_c = 0$). We also compute, for reference, a case without any forest ($F_c = 0$). The goal
615   is to evaluate how tropospheric WV transport and evapotranspiration alter precipitation distribution for
616   these two distinct environmental settings shown in Fig. 18a. We compute the solution at t=300 yrs for a
617   tropospheric dispersion of 10^4 m^2/s and no wind, thus providing equivalent normalized precipitation as
618   a function of coast-to-forest distance. The coastal forest case (Fig. 18b) reveals an efficient water transfer
619   from the ocean to the continent. Indeed, significant precipitation amounts are observed as far as 400 km
620   inside the continent due to the forested zone providing high evapotranspiration, the annual precipitation
621   of the coastal area being in the range 0.8-1m, dramatically larger than the one associated to a deforested
622   area (like the right coast of the model receiving only 0.05-0.1m). Although central forest is set to the
623   same spatial extension than coastal forest, the precipitation feed-back appears to be much weaker with
624   an average precipitation value of 0.2 m over the central forest (Fig. 18c).
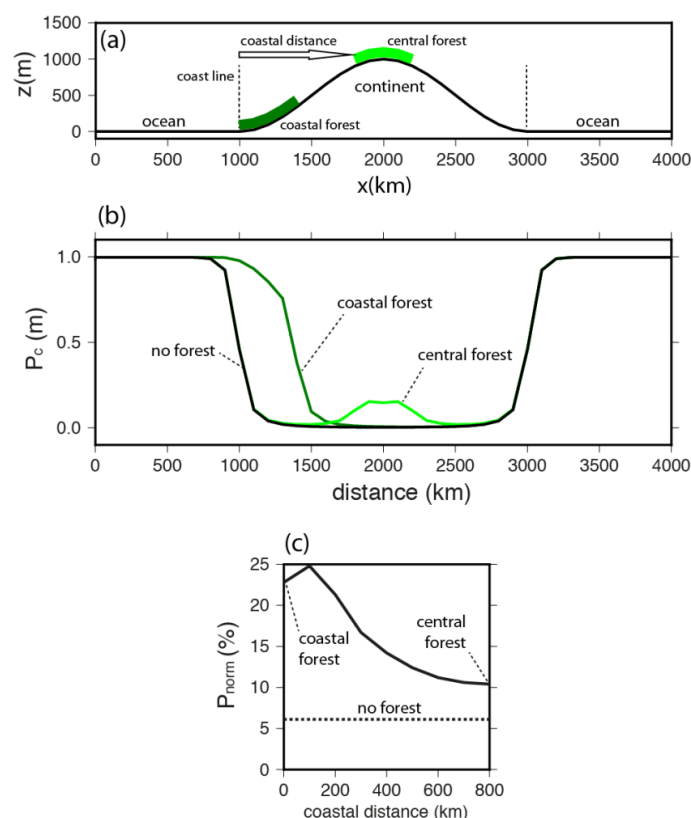625

Figure 18. (a) Location of respectively coastal and central forest cases (b) spatial precipitation distribution for no forest (black line), coastal forest (dark green curve) and central forest (light green curve) (c) average continental precipitation normalized by its oceanic counterpart as a function of coast-to-forest distance (solid curve) and for a non-forested area (dashed line)

5. Discussion

5.1 Parsimony model analysis

Water cycle experiments presented in the previous section embed four interconnected factors: (1) horizontal water vapor flow (2) liquid water production by condensation (3) horizontal groundwater flow (4) evapotranspiration by the vegetation. The idea that continental precipitation emerges as a combination of these dynamical processes is not new (Foley et al., 2003), but its quantitative exploration was until now restricted to the use of coupled atmospheric, hydrologic and vegetation models involving a high complexity level, thus rendering unreachable a user-friendly research. We mean by user-friendly that testing alternate constitutive equations, special boundary conditions and more generally new working hypothesis should be easy to perform in order to foster new discoveries. State-of-the-art meteorological codes, operable by specialized users on supercomputers, do not match this requirement.

By contrast, our parsimony model delivers fast-track continental precipitation simulations, opening doors to hundreds of ad-hoc models. This strategy allowed us to test numerous parameters associated to:
-   atmosphere (horizontal tropospheric dispersion, wind velocity, continental surface temperature);
-   biosphere (forest coverage ratio, potential evapotranspiration or ET);

651   -   lithosphere (topographic elevation, upper aquifer withdrawal time, lower aquifer hydraulic
652   conductivity).
653 Starting from empty atmosphere and underground water reservoirs, the three independent variables of
654 the model (WV concentration $C(x)$, upper and lower aquifer water height $h_{ua}(x)$ and $h_{la}(x)$, see table
655 1) dynamically evolve towards a steady state solution, meaning that incoming oceanic WV becomes
656 balanced by water exported by continental aquifers and surface runoff (Fig. 4).
657
658 Parameter's space exploration leads to the following propositions:
659   a.   when models embed limited biophysical activity (sparse forest and/or low potential ET), coastal
660   areas emerge as a damping zone for oceanic precipitation, the inner continent remaining dry.
661   This situation is clearly associated to a decay of WV concentration with a length scale depending
662   on the tropospheric dispersion. This result aligns with previous work (Ogino et al., 2017;
663   Yamanaka et al., 2018) describing the ocean/continent limit as a "coastal dehydrator", a concept
664   also illustrated by the relative humidity map of Australia (Fig. 2c).
665   b.   when dense forests and therefore high potential ET take place, precipitation extends inland if
666   the upper aquifer is able to fill. In our model, this implies that the lower aquifer can accumulate
667   enough water to overflow into upper aquifer. This condition initiates biophysical (forest) water
668   pumping and evapotranspiration, adding humidity to the atmosphere, resulting into dramatic
669   rainfall increase even in remote inland regions (Fig. 11a,b) compared to the case with sparse
670   forest (Fig. 10a,b). This result clearly supports MG2007 claim, stating that large forested areas
671   are the ultimate cause for large and homogeneous continental precipitation. However, the
672   underlying physical process for such a precipitation pattern is not the one invoked in MG2007
673   (in short: a wind induced by WV condensation over the forest). Rather, we rally a classical
674   meteorological view postulating that rain occurs by combining two processes: (1) forest
675   evapotranspiration that enriches tropospheric WV concentration (vertical flow) and (2)
676   tropospheric dispersion bringing oceanic moisture at large distance from its production area (3)
677   opposite groundwater fluxes balanced tropospheric WV dispersion. Starting from empty
678   aquifers, dynamic evolution take place over tens or hundreds of years thanks to regressive –
679   initiated along the coast – aquifers filling (Fig. 12).
680   c.   The contrasted rainfall distribution of these two situations (ie. function of forest coverage) above
681   is modulated by parameters related to topographic/atmospheric/hydrogeologic situations, also
682   including vegetation dynamics. Among these governing factors, topography and aquifer's
683   dynamics play a key role. Indeed, lowlands – as they exist in large tropical and boreal forests –
684   decrease underground Darcy's flow, thus favoring water accumulation in the continent, in turn
685   enhancing effective ET and WV concentration, finally triggering precipitation (Fig. 17b). Wind
686   is another factor that directly influences WV coming from oceanic domain in addition to
687   concentration gradient (see eq. 1). Through wind continent breaks the symmetry of
688   concentration, precipitation and runoff functions with respect to mid-continent divide. As
689   observed in natural situations (see the Australian case of Fig. 2), upwind coasts then receive
690   more precipitation that their downwind counterpart (Fig. 16), due to a combination of WV
691   concentration asymmetry and orographic effect (which is not modelled here, see comment about
692   eq. 2).
693
694 5.2 Tropospheric dispersion length scale
695
696   The precipitation decay from ocean to continent (see Fig. 10b) can directly be linked to model's
697 parameters if atmospheric equations are condensed into a single expression. Such a compact formulation
698 can be written when considering the steady state form of eq. 1 and a linear form of eq. 4 ($n = 1$). Then,
699 equations 1, 3 and 4 provide a second order differential equation with constant coefficients:
700
701 $D_h \frac{d^2C}{dx^2} - v\frac{dC}{dx} + \frac{1}{t_{rain}}C = \frac{\rho_w g}{P_{atm}}\dot{E}$ (eq. 12)

702

703 $\dot{E}$ being equal to zero and 1m/yr over oceanic and continental domains, respectively. Due to the linearity
704 of eq. 4, solutions of $C(x)$, $\dot{P}(x)$ and cumulated precipitation $P_c(x)$ are homothetic and can be
705 explicitly written as the sum of two exponential functions (see Appendix A for demonstration):
706

707 $$C(x) = c_1 e^{\lambda_1 x} + c_2 e^{\lambda_2 x} + \frac{\rho_w g}{P_{atm}} t_{rain}\dot{E} \qquad\qquad \text{(eq. 13)}$$
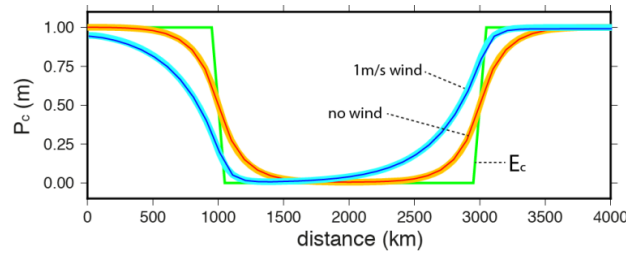
708

709
710 *Figure 19. Spatial precipitation distribution associated to eq. 12. Green curve represents evaporation*
711 *profile (right hand side of eq. 12). Bold curves (orange= no wind; cyan= -1m/s wind) are associated*
712 *to analytical solutions (eq. 13) while thin curves (red=no wind; blue=-1m/s wind) correspond to*
713 *numerical solutions after 100yrs.*
714

715 We compute this function (eq. 13) using an evaporation E_c of 1m on the ocean, a null
716 evapotranspiration on the continent, a dispersion D_h of 10^5 m²/s, a time scale t_{rain} of 3 days and two
717 wind values: $v = 0$ and a wind coming from east at 1 m/s. Comparing analytical and numerical solutions
718 (Fig. 20) lead to an excellent agreement for $n = 1$. In the case of a null wind, $\lambda_1 = \lambda_2$ and eq. 13
719 provides a simple expression of the characteristic damping distance of the solution:
720

721 $$\sigma = 1/\lambda_1 = \sqrt{D_h t_{rain}} \qquad\qquad \text{(eq. 14)}$$

722

723 Using modeling value of t_{rain} (3 days, see Table 1), damping distances of 16, 50 and 161 km are found
724 for respectively atmospheric dispersion values of 10^3, 10^4 and 10^5 m²/s. The above relationships (eq. 13
725 and 14, fig. 20) may support the conclusion of Ogino et al (2017) concerning dehydration processes with
726 a characteristic wavelength of 150 km. Indeed, these authors state that "*the dehydration process robustly*
727 *exists as a global mean feature over a range of a few hundred kilometers from the coastline*". Therefore,
728 this dehydration length may correspond to the damping distance definition given by eq. 14 (null average
729 wind) corresponding to $E > P_c$ over oceanic domain while to $E < P_c$ on continental areas.
730

731 5.3 Forest physiology evolution and continental colonization
732

733 We implemented a formulation allowing to convert potential evapotranspiration rate (ET_p) to real
734 evapotranspiration rate $\dot{E}$, this latter quantity being tuned by available underground water for root uptake
735 (eq 7a,b). However, we did not consider other physiological factors controlling biophysical forest
736 dynamics. Three of them matter as far as climate change is concerned:
737 The first one is associated to the proposition that "*actual rooting depths reflect ecologically*
738 *optimized responses to weather and climate variability*" (Feddes et al., 2001), as reviewed by Bachofen
739 et al. 2024. For example, Mediterranean tree species develop deep root systems (more than 10 m depth)
740 to survive during summer droughts with a root/shoot ratio increase toward drier conditions (Cabon et
741 al., 2018), following the eco hydrological equilibrium theory (Eagleson, 1982). Following this theory,
742 leaf area index, driving transpiration, also adjusts to dry conditions (Hoff and Rambal, 2003).
743 The second one is that forests are self-organized, species diversity promoting global forest
744 productivity (Morin et al, 2025). These two factors play at time scales associated to individual trees
745 lifetime and also the time needed to obtain a mature forest, meaning hundreds of years depending on
746 climate conditions. This suggests that forests are optimized to uptake water from shallow aquifers, both

25

747 individually and collectively, with complementary strategies between species leveraging the trade-off
748 between root depth and drought tolerance (Brum et al. 2019). Because these two factors are likely to
749 influence evapotranspiration amplitude and seasonality, large forests should modify climate through
750 physical processes that we have described and modelled.

751 In addition, a very long-term factor may influence climate and precipitation distribution at
752 geological time scales: continental life evolution started from small plants species to evolve towards
753 large trees. We know from geological records that the first episode of forest spreading occurred at
754 Devonian times (420 to 360 My bp) along with a massive transition of plant physiology, climate and
755 hydrology Gess and Berry (2024). Quoting from these authors, "*Devonian was a time of significant
756 evolution of plant life, with the establishment of forest stature vegetation for the first time in Earth
757 history. This development is believed to have had massive permanent repercussions; enhancing the
758 chemical weathering of rocks, changing the nature of fluvial systems…*". Among various emerging
759 physiological factors, the dramatic increase of both plant size and root system is of specific interest to
760 understand the link between plant evolution and climate change (Fan et al., 2017; Stein et al., 2020;
761 Laughlin et al., 2021).

762 To build a retroactive mechanism between forest development and precipitation distribution, we
763 consider that plant development physiological factors are solar powered. First, a large part of this
764 radiative power is absorbed or re-emitted as heat flux in infrared energy bandwidth, the thermoregulation
765 being achieved by latent heat release by plant transpiration (Zeng & Zhang, 2020). This process is partly
766 modeled here (plant transpiration) by using solar radiation as a parameter (eq. 4). Secondly, a small part
767 of solar energy is used to create organic matter by photosynthesis. It would be useful to model this
768 second process in the framework of our model and to setup a plant growth function to complement
769 evapotranspiration function. Such a coupling between forest dynamics and global water cycle may lead
770 to the following 3-phase scenario:

    a. Devonian time shelfs (Laurassia and Gondwana) presented a large extension similar to those
       of our modern continents. Prior to forest development, plates interiors were likely to be free
       of massive evapotranspiration sources. In such a case, our models indicate that large
       precipitation should have been limited to coastal areas, remaining inland zones dry.

    b. Triggered by coastal rain, trees growth and initial forest development should have therefore
       started along the coast, species equipped by deep root systems being favored in order to
       penetrate inside continents. Looking to Fig. 3 of Gess and Berry (2020), *Archaeopteris* paleo-
       trees are found in such paleogeographic position. During this initial spreading, precipitation
       patterns of forests invading coastal areas should resemble to the transition from black to dark
       green curve of Fig. 18b. This suggests that rainfall migrates inland as forests growth and
       aquifers fill.

    c. As forest colonization goes on, its rate is modulated by some factors that we modeled: wind,
       topography and temperature, and others like soil weathering rate, plant growing rate,
       mortality rate and other geological factors. Depending on their influence, forest may have
       spread partially or totally over continents due to the positive combination of four factors: WV
       horizontal transfer, forest evaporative function, precipitation enhancement and aquifers
       filling. This interplay may have induced major climatic shifts during Earth evolution, the
       fundamental pattern being that forest colonization may extend inland by converting dry
       shelves interiors to humid and rainy continents (see Fig. 11b).

791 5.4 Holocene climate, forests and civilization fate

793 The end of Mediterranean Holocene humid period around 6500 years ago is generally attributed
794 to an astronomical forcing inducing monsoon migration (e.g. Marzin et Braconnot, 2009). However,
795 these interpretations remain speculative because climate model's predictions are not backed by direct
796 paleo-meteorological observations. Because Mediterranean and African deforestation took place during
797 Holocene times, it has also been suggested that a climate modification by human societies might also
798 have occurred, thus hasting the end of African humid period (Wright, 2017). As an alternate view to
799 astronomical forcing, our model supports the proposition that human societies may have lowered

800 precipitation by massive forest clearance, thus depleting aquifers. This hypothesis is supported by the
801 fact that time scales associated to natural forest growth are of hundreds of years, implying that present-
802 day databases are not long enough to display this slow balance evolution. Despite youngly afforested
803 zones may not display obvious meteorological or hydrologic changes (Douville et al., 2024), some
804 studies suggest that this effect is already detectable (e.g. Li et al., 2021). The second element supporting
805 our hypothesis is that deforestation is systematically associated to rainfall decrease and droughts at any
806 latitude and climate (Perugini et al., 2017; Smith et al., 2023).

807   Contrary to fossil fuel extraction, man induced deforestation started a long time ago but this
808 tendency accelerates at the dawn of Holocene (Williams, 2003) because of two novel factors: animal
809 domestication and cultivated plants spreading. Both activities exerted a direct pressure on forests that
810 have been converted to pasture and grain fields. Some retroactive effects of these changes are well
811 known: food productivity increase, soil erosion and biodiversity drop. Since these effects are visible in
812 many ancient societies since 10 000 years BC, their climatic and hydrologic consequences may have
813 challenged their survival.

814   Although social and political causes are *in-fine* responsible for instabilities and tragic fates of
815 civilizations, we propose that a physical factor also undermines mankind stability during Holocene
816 times: precipitation decay and droughts due to forest conversion to pasture and cereals fields. To
817 understand how this may occur, we start from one of our model's output: continental rain is tuned by
818 two main parameters: moisture brought by dispersion and oceanic wind and local evapotranspiration.
819 We also need to considerate processes associated to vegetation that are seasonal and largely tuned by
820 temperature and plant physiology. Therefore, grain fields display large evapotranspiration during their
821 growing time and then decline in summer. More specifically, harvest abruptly ends evapotranspiration,
822 inducing sharp decrease of atmospheric humidity. This process is occurring also for plants reproducing
823 by seeds with summer drying up.

824   Despite we did not explicitly model these seasonal variations, further use of our model may help
825 exploring the relation between ending of evapotranspiration and summer precipitation decay, leading to
826 progressive aquifer depletion. Repeated over decades, long and dry summers may have shifted the time
827 of dry period to middle or early spring, therefore increasing the probability of crop failures, adding
828 starvation to rain shortage. The negative impact of natural forests to pasture or culture conversion on
829 precipitation may also sums up with ground level temperature increase induced by evapotranspiration
830 drop (latent heat effect). We propose that replacing forest by crops may have drastically decrease annual
831 precipitation thus favoring societal disorders. Because water resources and associated cultural practices
832 were vital for ancient Mediterranean societies, decays of some prehistoric societies (Vidale et al., 2018)
833 and the collapse of Bronze age (Vaezi et al., 2022; Cline, 2021) might have been caused by man-induced
834 climate change.

835
836 5.5 Implications for land and forest management
837

838   The lack of a general acknowledgment of the forest - precipitation retroaction has multiple origins,
839 one of them being the belief that moisture advection by wind stands as the most efficient way to transport
840 oceanic moisture over continent. This interpretation is certainly true for areas presenting a polarized
841 annual wind budget like coasts facing trade winds or westerlies. In such a case, it is likely that forests
842 should cause minor change to precipitation budget and vegetation must adapt to the meteorological
843 forcing.

844   The situation appears to be different when wind budget is close to zero, implying that dispersion
845 effect plays a key role: moisture gradient invariably transfers WV from a wet ocean to a drier continent
846 (see eq. 1). In such a case, forest evapotranspiration may stimulate precipitation in two ways: (1)
847 bringing WV concentration to its condensation limit, and (2) decreasing lower troposphere temperature
848 by evapotranspiration. We also have seen that specific geographic configurations – like coastal forests
849 – maximize inland precipitation (Fig. 18). Because Neolithic and historical migrations preferentially
850 followed coastal routes all around the world, coastal areas have been more or less constantly deforested.
851 As a result, long term man induced deforestation – for example in the Mediterranean basin – may have
852 severely altered regional precipitation regimes. We may therefore conjecture that the natural equilibrium
853 state of large geographic zones (ie, forest extension and precipitation that would have occurred without
854 man interaction) is completely unknown.

855 Completing existing works on the beneficial ecological role of forests (Singh et al., 2024; Bastin
856 et al., 2019), our model brings theoretical support to the conjecture that forests enhance precipitation
857 (Hoek et al., 2022, Makarieva et al., 2023, Yang et al., 2023). We raise an important factor that may
858 have been underestimated in the past: the magnitude of the retroaction fully depends on the hydrological
859 part of the global water cycle system. Indeed, it is well known that forests are pumping into aquifers,
860 thus increasing the risk of drying sources and decreasing river flows (Zhang et al, 2008) if precipitation
861 remains constant. But we have seen that this latter assumption is flawed: atmospheric WV transport,
862 vegetation activity and aquifer dynamics are fully coupled. This physical entanglement implies that three
863 scientific communities – dynamic meteorology – forest ecology – hydrology – must work together to
864 define new climatic scenarios. This occurs at a special time when climate projections predict
865 precipitation decrease, aquifers depletion and drought increase over many continental areas (Tramblay
866 et al., 2020). This scenario appears to be paradoxical if we consider the physical origin of precipitation:
867 temperature increase means more sea evaporation, thus more rain available over neighboring countries
868 if moisture is transported there and condensates. Such a warming/greening/wetting scenario has been
869 recently revealed by paleobotanists for a hot Miocene period in South America (Ochoa et al., 2025). Our
870 modeling results indicate that such evolution could be systemic, and that natural afforestation should be
871 an efficient and ecological way to reactivate precipitation around large evaporative bodies.
872
873 **6. Conclusion**
874
875 The conjecture that "*forests favor continental scale pluviometry*" received various appreciations
876 along historic periods. Early observers (Christopher Colombus back to sixteenth century, many eighteen
877 century engineers and foresters) acknowledged that forests trigger pluviometry thanks to *de visu*
878 observations, while modern science mostly ignores or disagrees with this opinion. It is interesting to
879 notice that the revival of this proposition by Makarieva and Gorshkov (2007) – stating that forests induce
880 precipitation – was either received positively or negatively depending on scientific community. Most of
881 positive comments came from forest ecology community (eg. Sheil & Murdiyarso, 2009), while
882 hydrology community considered this conjecture as not outrageous (Wierik et al., 2021), probably
883 because the impact of deforestation on rainfall decay is clearly demonstrated by data. By contrast,
884 meteorology and climatology literature did not explore this conjecture, assuming that the underlying
885 physical explanation of MG2007 is flawed (Meesters et al., 2009).
886 Through this work, we have shown that the proposition "*forests favor continental scale
887 pluviometry*" has far reaching digitations: basic meteorological equations, forest physiology,
888 root/aquifer interactions at different scales, underground water flow. Its overall formulation is so
889 complex that its understanding is unbearable by reductionist scientific practices that have been
890 developed during several decades and that form the overwhelming majority of modern scientific papers.
891 A proper formulation – tractable and understandable – requires a double move: (1) a holistic shift, to
892 consider together in a unified physical formalism all aspects of the water cycle beyond the ideal view of
893 Fig. 3, and (2) a parsimony strategy, to define an adequate simplification of the problem, facing the need
894 to remain in contact with observations. In our attempt to tackle the "biotic pump" problem defined by
895 MG2007, we have formulated a parsimony model that explain that "*forests favor continental scale
896 pluviometry*" under certain conditions. Considering that the physical mechanisms of the retroaction have
897 been presented for the first time in the present paper, we hope that this work will induce further research
898 with the practical goal of avoiding a dry future for many populations.
899
900 **7. Appendix A**
901
902 We consider the equation:
903
904 $$D\ C'' - vC' - \alpha C = A \qquad\qquad (A1)$$
905
906 With $\alpha > 0$, with a computing domain ranging from $0\ to\ 4L$. The solution is split into 3 branches: C_1
907 for x < L, C_2 for L<x<3L, C3 for 3L<x<4L. The source A is constant over each of these domains. We
908 apply homogeneous Neumann conditions at the boundaries for x=0 and x=4L:
909

910 $C_1'(0) = 0$, $C_3'(4L) = 0$ (A2)
911
912 And we also impose the continuity of the solution and its derivatives to ocean-continent transitions:
913
914 $C_1 (L) = C_2 (L)$, $C_1'(L) = C_2'(L)$ (A3)
915 $C_2 (3L) = C_3 (3L)$, $C_2'(3L) = C_3'(3L)$ (A4)
916
917 We consider a negative wind ($v < 0$) and we choose *a-posteriori* the solution that corresponds to a null
918 derivative for x=0 and x=4L, with setting value of C for x=4L (incoming moisture flow). The
919 characteristic equation of eq. A1 is given by:
920
921 $D \ \lambda^2 - v\lambda \ - \alpha = 0$ (A5)
922
923 that corresponds to the following real solutions:
924
925 $\lambda_{1,2} = \frac{v \pm \sqrt{v^2 + 4D\alpha}}{2D}$ (A6)
926
927 The general solution is given by:
928
929 $C(x) = c_1 e^{\lambda_1 x} + c_2 e^{\lambda_2 x} - A/\alpha$ (A7)
930
931 The constants c_1 and c_2 being computed for each region using boundary conditions and ocean-continent
932 transitions values by solving a 6x6 linear system.
933
934 **8. Code availability**
935
936 The code used for this work and corresponding input files are available on request to the corresponding
937 author.
938
939 **9. Data availability**
940
941 The datasets analysed during the current study are available in the NSF NCAR Research Data Archive
942 (RDA) repository, https://rda.ucar.edu/datasets/d628001/ for the JRA-55 data, and in the Global Land
943 Analysis and Discovery (GLAD) laboratory at the University of Maryland
944 repository, https://storage.googleapis.com/earthenginepartners-hansen/GFC-2023-
945 v1.11/download.html
946 for the Global Forest Change data.
947
948 **10. Author contributions**
949
950 All authors contributed to the study conception and design. Model conception, programmation,
951 numerical experiments and a first version of the manuscript were performed by JC. Material preparation,
952 data collection and data analysis were performed by MP while BM provided analytical solutions
953 provided in the paper. CC reviewed the links between different fields: meteorology, forest and
954 underground hydrology. All authors commented on previous versions of the manuscript, read and
955 approved the final manuscript.
956
957 **11. Competing Interests**
958
959 The authors have no relevant financial or non-financial interests to disclose.
960
961 **12. Acknowledgments**
962

14. References

Alexandris, S., & Kerkides, P. (2003). New empirical formula for hourly estimations of reference evapotranspiration. *Agricultural Water Management*, *60*(3), 157-180.

Asselin, O., Leduc, M., Paquin, D., de Noblet-Ducoudré, N., Rechid, D., & Ludwig, R. (2024). Blue in green: forestation turns blue water green, mitigating heat at the expense of water availability. *Environmental Research Letters*, *19*(11), 114003.

Andréassian, V. (2004). Couvert forestier et comportement hydrologique des bassins versants. *La houille blanche*, *90*(2), 31-35.

Bachofen, C., Tumber-Dávila, S. J., Mackay, D. S., McDowell, N. G., Carminati, A., Klein, T., ... & Grossiord, C. (2024). Tree water uptake patterns across the globe. *New Phytologist*, *242*(5), 1891-1910.

Bastin, J. F., Finegold, Y., Garcia, C., Mollicone, D., Rezende, M., Routh, D., ... & Crowther, T. W. (2019). The global tree restoration potential. *Science*, *365*(6448), 76-79.

Bochow, N., & Boers, N. (2023). The South American monsoon approaches a critical transition in response to deforestation. *Science Advances*, *9*(40), eadd9973.

Brum, M., Vadeboncoeur, M. A., Ivanov, V., Asbjornsen, H., Saleska, S., Alves, L. F., ... & Oliveira, R. S. (2019). Hydrological niche segregation defines forest structure and drought tolerance strategies in a seasonal Amazon forest. *Journal of Ecology*, *107*(1), 318-333.

Cabon, A., Martínez-Vilalta, J., Martinez de Aragon, J., Poyatos, R., & De Cáceres, M. (2018). Applying the eco-hydrological equilibrium hypothesis to model root distribution in water-limited forests. *Ecohydrology*, *11*(7), e2015.

Cline, E. H. (2021). 1177 BC: The Year Civilization Collapsed: The Year Civilization Collapsed. In *1177 BC: The Year Civilization Collapsed*. Princeton University Press.

Dakos, V., Boulton, C. A., Buxton, J. E., Abrams, J. F., Arellano-Nava, B., Armstrong McKay, D. I., Bathiany, S., Blaschke, L., Boers, N. …. and Kéfi, S. (2024) Tipping point detection and early warnings in climate, ecological, and human systems, Earth Syst. Dynam., 15, 1117–1135.

Descroix, L., & Barrios, J. L. (2001). et Solis, R. Influence de la forêt sur la pluviométrie. *La Sierra Madre Occidentale, un Château d'eau menacé ; IRD Edition: Paris, France*, 239.

Douville, H., Allan, R. P., Arias, P. A., & Fisher, R. A. (2024). Call for caution regarding the efficacy of large-scale afforestation and its hydrological effects. *Science of The Total Environment*, 175299.

Drobinski, P., Alonzo, B., Bastin, S., Silva, N. D., & Muller, C. (2016). Scaling of precipitation extremes with temperature in the French Mediterranean region: What explains the hook shape?. *Journal of Geophysical Research: Atmospheres*, *121*(7), 3100-3119.

Ebita, A., Kobayashi, S., Ota, Y., Moriya, M., Kumabe, R., Onogi, K., Harada, Y., Yasui, S., Miyaoka, K., Takahashi, K., Kamahori, H., Kobayashi, C., Endo, H., Soma, M., Oikawa, Y., & Ishimizu, T., (2011). The Japanese 55-year Reanalysis "JRA-55": an interim report, SOLA, 7, 149-152.

Eagleson, P.S. (1982) Ecological optimality in water-limited natural soil-vegetation systems. 1. Theory and hypothesis. Water Resources Research 18, 325–340.

El Idrysy, E. H., & De Smedt, F. (2007). A comparative study of hydraulic conductivity estimations using geostatistics. *Hydrogeology Journal*, *15*, 459-470.

Eltahir, E. A. (1998). A soil moisture–rainfall feedback mechanism: 1. Theory and observations. *Water resources research*, *34*(4), 765-776.

Fan, Y., Miguez-Macho, G., Jobbágy, E. G., Jackson, R. B., & Otero-Casal, C. (2017). Hydrologic regulation of plant rooting depth. *Proceedings of the National Academy of Sciences*, *114*(40), 10572-10577.

Feddes, R. A., Hoff, H., Bruen, M., Dawson, T., De Rosnay, P., Dirmeyer, P., ... & Pitman, A. J. (2001). Modeling root water uptake in hydrological and climate models. *Bulletin of the American meteorological society*, *82*(12), 2797-2810.

Filimonova, M., & Trubetskova, M. (2005). Calculation of evaporation from the Caspian Sea surface. In *9th ISSH SEMINAR on Stochastic Hydraulics, De Vereeniging, Nijmegen, The Netherlands* (pp. 23-24).

Fleury, P., Plagnes, V., & Bakalowicz, M. (2007). Modelling of the functioning of karst aquifers with a reservoir model: Application to Fontaine de Vaucluse (South of France). *Journal of hydrology*, *345*(1-2), 38-49.

1022 Foley, J. A., Costa, M. H., Delire, C., Ramankutty, N., & Snyder, P. (2003). Green surprise? How terrestrial
1023   ecosystems could affect earth's climate. *Frontiers in Ecology and the Environment*, *1*(1), 38-44.
1024 Fressoz, J. B. (2020). Les politiques de la nature au début de la révolution. Sens et fonctions de l'alerte
1025   environnementale, 1789-1793. In *Annales historiques de la Révolution française*, 1, 19-38.
1026 Gess, R. W., & Berry, C. (2024). Archaeopteris trees at high southern latitudes in the late Devonian. *Review of
1027   Palaeobotany and Palynology*, *331*, 105212.
1028 Gimeno, L., Stohl, A., Trigo, R. M., Dominguez, F., Yoshimura, K., Yu, L., ... & Nieto, R. (2012). Oceanic and
1029   terrestrial sources of continental precipitation. *Reviews of Geophysics*, *50*(4).
1030 Hansen, M. C., Potapov, P. V., Moore, R., Hancher, M., Turubanova, S. A., Tyukavina, A., Thau, D., Stehman,
1031   S. V., Goetz, S. J., Loveland, T. R.,Kommareddy, A., Egorov, A., Chini, L., Justice, C. O., &
1032   Townshend, J. R. G. (2013). High-Resolution Global Maps of 21st-Century Forest Cover Change.
1033   *Science*, 342, 850-53.
1034 Harrison, S. P., Cramer, W., Franklin, O., Prentice, I. C., Wang, H., Brännström, Å., ... & Wright, I. J. (2021).
1035   Eco-evolutionary optimality as a means to improve vegetation and land-surface models. *New
1036   Phytologist*, *231*(6), 2125-2141.
1037 Hoek van Dijke, A. J., Herold, M., Mallick, K., Benedict, I., Machwitz, M., Schlerf, M., ... & Teuling, A. J.
1038   (2022). Shifts in regional water availability due to global tree restoration. *Nature Geoscience*, *15*(5),
1039   363-368.
1040 Hoff, C., & Rambal, S. (2003). An examination of the interaction between climate, soil and leaf area index in a
1041   Quercus ilex ecosystem. *Annals of Forest Science*, *60*(2), 153-161.
1042 Hubbert, M. K. (1956). Darcy's law and the field equations of the flow of underground fluids. *Transactions of
1043   the AIME*, *207*(01), 222-239.
1044 Ishikawa, H. (1995). Evaluation of the effect of horizontal diffusion on the long-range atmospheric transport
1045   simulation with Chernobyl data. *Journal of Applied Meteorology and Climatology*, *34*(7), 1653-1665.
1046 Jacob, T., Chery, J., Bayer, R., Le Moigne, N., Boy, J. P., Vernant, P., & Boudin, F. (2009). Time-lapse surface
1047   to depth gravity measurements on a karst system reveal the dominant role of the epikarst as a water
1048   storage entity. *Geophysical Journal International*, *177*(2), 347-360.
1049 Läderach, A., & Sodemann, H. (2016). A revised picture of the atmospheric moisture residence time.
1050   *Geophysical Research Letters*, *43*(2), 924-933.
1051 Laio, F., Porporato, A., Ridolfi, L., & Rodriguez-Iturbe, I. (2001). Plants in water-controlled ecosystems: active
1052   role in hydrologic processes and response to water stress: II. Probabilistic soil moisture dynamics.
1053   *Advances in water resources*, *24*(7), 707-723.
1054 Läderach, A., & Sodemann, H. (2016). A revised picture of the atmospheric moisture residence time.
1055   *Geophysical Research Letters*, *43*(2), 924-933.
1056 Laughlin, D.C., Mommer, L., Sabatini, F.M. *et al.* (2021) Root traits explain plant species distributions along
1057   climatic gradients yet challenge the nature of ecological trade-offs. *Nat Ecol Evol* **5**, 1123–1134.
1058 Le Pichon, X. (1968). Sea-floor spreading and continental drift. *Journal of geophysical research*, *73*(12), 3661-
1059   3697.
1060 Li, W., Li, L., Chen, J., Lin, Q., and Chen, H.(2021) Impacts of land use and land cover change and reforestation
1061   on summer rainfall in the Yangtze River basin, Hydrol. Earth Syst. Sci., 25, 4531–4548.
1062 Lorenz, E. N. (1963). Deterministic nonperiodic flow. *Journal of atmospheric sciences*, *20*(2), 130-141.
1063 Maillet, E. T. (1905). *Essais d'hydraulique souterraine & fluviale*. A. Hermann.
1064 Makarieva, A. M., & Gorshkov, V. G. (2007). Biotic pump of atmospheric moisture as driver of the hydrological
1065   cycle on land. *Hydrology and earth system sciences*, *11*(2), 1013-1033.
1066 Makarieva, A. M., Nefiodov, A. V., Rammig, A., & Nobre, A. D. (2023). Re-appraisal of the global climatic role
1067   of natural forests for improved climate projections and policies. *Frontiers in Forests and Global
1068   Change*, *6*, 1150191.
1069 Marzin, C., & Braconnot, P. (2009). Variations of Indian and African monsoons induced by insolation changes
1070   at 6 and 9.5 kyr BP. *Climate Dynamics*, *33*(2), 215-231.
1071 McKenzie, D. (1978). Some remarks on the development of sedimentary basins. *Earth and Planetary science
1072   letters*, *40*(1), 25-32.
1073 Meesters, A. G. C. A., Dolman, A. J., & Bruijnzeel, L. A. (2009). Comment on" Biotic pump of atmospheric
1074   moisture as driver of the hydrological cycle on land" by AM Makarieva and VG Gorshkov, Hydrol.
1075   Earth Syst. Sci., 11, 1013–1033, 2007. *Hydrology and Earth System Sciences*, *13*(7), 1299-1305.
1076 Monteith, J. L. (1965). Evaporation and environment. In *Symposia of the society for experimental biology* (Vol.
1077   19, pp. 205-234). Cambridge University Press (CUP) Cambridge.
1078 Morin, X., Toigo, M., Fahse, L., Guillemot, J., Cailleret, M., Bertrand, R., ... & Vallet, P. (2025). More species,
1079   more trees: The role of tree packing in promoting forest productivity. *Journal of Ecology*.
1080 Morgan, W. J. (1968). Rises, trenches, great faults, and crustal blocks. *Journal of Geophysical Research*, *73*(6),
1081   1959-1982.

1082   <u>Mouillot F.</u> & Field C.B. (2005). Fire history and the global carbon budget : a 1 degrees x 1 degrees fire history
1083   reconstruction for the 20th century. *Global Change Biology*, 11 (3), p. 398-420.
1084   Neelin, J. D., Peters, O., & Hales, K. (2009). The transition to strong convection. *Journal of the Atmospheric*
1085   *Sciences*, *66*(8), 2367-2384.
1086   Niedorf, A., Finkensieper, S., Konrad, H, Roca, R., Schröder, M., Cloché, S., Panegrossi, G., Sanò, P., Kidd, C.,
1087   Jucá Oliveira, R. A., Fennig, K., Sikorski, T., … & Hollmann, R. (2024). GIRAFE v1: CM SAF Global
1088   Interpolated RAinFall Estimation version 1, Satellite Application Facility on Climate Monitoring.
1089   Nobre A. (2007). Interactive comment on "Biotic pump of atmospheric moisture as driver of the hydrological
1090   cycle on land" by AM Makarieva and VG Gorshkov. *Hydrology and Earth System Sciences*
1091   *Discussions*, *3*, S1176-S1184.
1092   Ntona, M. M., Busico, G., Mastrocicco, M., & Kazakis, N. (2022). Modeling groundwater and surface water
1093   interaction: An overview of current status and future challenges. *Science of the Total Environment*, *846*,
1094   157355.
1095   Ochoa, D., Carré, M., Montenegro, J. F., DeVries, T. J., Caballero-Rodríguez, D., Rodríguez-Reyes, O., ... &
1096   Flores, J. A. (2025). Late Miocene greening of the Peruvian Desert. *Communications Earth &*
1097   *Environment*, *6*(1), 1-12.
1098   Ogino, S. Y., Yamanaka, M. D., Mori, S., & Matsumoto, J. (2017). Tropical coastal dehydrator in global
1099   atmospheric water circulation. *Geophysical Research Letters*, *44*(22), 11-636.
1100   Paço, T. A., David, T. S., Henriques, M. O., Pereira, J. S., Valente, F., Banza, J., ... & David, J. S. (2009).
1101   Evapotranspiration from a Mediterranean evergreen oak savannah: the role of trees and pasture. *Journal*
1102   *of Hydrology*, *369*(1-2), 98-106.
1103   Penman, H. L. (1948). Natural evaporation from open water, bare soil and grass. *Proceedings of the Royal*
1104   *Society of London. Series A. Mathematical and Physical Sciences*, *193*(1032), 120-145.
1105   Perugini, L., Caporaso, L., Marconi, S., Cescatti, A., Quesada, B., de Noblet-Ducoudré, N., ... & Arneth, A.
1106   (2017). Biophysical effects on temperature and precipitation due to land cover change. *Environmental*
1107   *Research Letters*, *12*(5), 053002.
1108   Pisso, I., Real, E., Law, K. S., Legras, B., Bousserez, N., Attié, J. L., & Schlager, H. (2009). Estimation of
1109   mixing in the troposphere from lagrangian trace gas reconstructions during long-range pollution plume
1110   transport. *Journal of Geophysical Research: Atmospheres*, *114* (D19).
1111   Rambal, S. (2015). Relations entre couverts végétaux des parcours et cycle de l'eau. *L'eau des troupeaux en*
1112   *alpages et sur parcours: une ressource à gérer, aménager, partager*, 25-37.
1113   Rasmusson, E. M. (1968). Atmospheric water vapor transport and the water balance of North America: II. Large-
1114   scale water balance investigations. *Monthly Weather Review*, *96*(10), 720-734.
1115   Reitan, C. H. (1963). Surface dew point and water vapor aloft. *Journal of Applied Meteorology (1962-1982)*,
1116   776-779.
1117   Sampaio, G., Nobre C.A., Costa, M.H., Satyamurty, Soares-Filho, P.B.S., Cardoso, M. (2007). Regional climate
1118   change over eastern Amazonia caused by pasture and soybean cropland expansion. *Geophys. Res. Lett.*
1119   **34**, L17709.
1120   Serrano, A., & Valbuena, J. (2017). Production and consumption-based water dynamics: A longitudinal analysis
1121   for the EU27. *Science of The Total Environment*, *599*, 2035-2045.
1122   Shoaee, M. J., Breeze, P. S., Drake, N. A., Hashemi, S. M., Nasab, H. V., Breitenbach, S. F., ... & Petraglia, M.
1123   D. (2023). Defining paleoclimatic routes and opportunities for hominin dispersals across Iran. *Plos one*,
1124   *18*(3).
1125   Singh, R. S., Prakash, O. P., & Khicher, M. L. (1995). Estimation of evaporation from different meteorological
1126   parameters. *Annals of Arid Zone*, *34*, 263-266.
1127   Singh, B., Jeganathan, C., Rathore, V. S., Atkinson, P. M., Behera, M. D., Singh, C. P., ... & Roy, P. S. (2024).
1128   The relationship between central Indian terrestrial vegetation and monsoon rainfall distributions in
1129   different hydroclimatic extreme years using time-series satellite data. *Theoretical and Applied*
1130   *Climatology*, *155*(1), 45-69.
1131   Sheil, D., & Murdiyarso, D. (2009). How forests attract rain: an examination of a new hypothesis. *Bioscience*,
1132   *59*(4), 341-347.
1133   Smith, C., Baker, J. C. A., & Spracklen, D. V. (2023). Tropical deforestation causes large reductions in observed
1134   precipitation. *Nature*, *615*(7951), 270-275.
1135   Steffen, W., Richardson, K., Rockström, J., Cornell, S. E., Fetzer, I., Bennett, E. M., ... & Sörlin, S. (2015).
1136   Planetary boundaries: Guiding human development on a changing planet. *science*, *347*(6223), 1259855.
1137   Stein, W. E., Berry, C. M., Morris, J. L., Hernick, L. V., Mannolini, F., Ver Straeten, C., ... & Leake, J. R.
1138   (2020). Mid-Devonian Archaeopteris roots signal revolutionary change in earliest fossil forests. *Current*
1139   *biology*, *30*(3), 421-431.

1140   Tiesi, A., Villani, M. G., D'Isidoro, M., Prata, A. J., Maurizi, A., & Tampieri, F. (2006). Estimation of
1141   dispersion coefficient in the troposphere from satellite images of volcanic plumes: Application to Mt.
1142   Etna, Italy. *Atmospheric Environment*, *40*(4), 628-638.
1143   Tramblay, Y., Koutroulis, A., Samaniego, L., Vicente-Serrano, S. M., Volaire, F., Boone, A., ... & Polcher, J.
1144   (2020). Challenges for drought assessment in the Mediterranean region under future climate scenarios.
1145   *Earth-Science Reviews*, *210*, 103348.
1146   Vaezi, A., Routh, J., Djamali, M., Gurjazkaite, K., Tavakoli, V., Beni, A. N., & Roberts, P. (2022). New multi-
1147   proxy record shows potential impacts of precipitation on the rise and ebb of Bronze Age and imperial
1148   Persian societies in southeastern Iran. *Quaternary Science Reviews*, *298*, 107855.
1149   Vargas Godoy, M. R., Markonis, Y., Hanel, M., Kyselý, J., & Papalexiou, S. M. (2021). The global water cycle
1150   budget: A chronological review. *Surveys in Geophysics*, *42*(5), 1075-1107.
1151   Van Dam, J. C., & Feddes, R. A. (2000). Numerical simulation of infiltration, evaporation and shallow
1152   groundwater levels with the Richards equation. *Journal of hydrology*, *233*(1-4), 72-85.
1153   Vidale, M., Fazeli-Nashli, H., & Desset, F. (2018). The late prehistory of the northern Iranian Central Plateau (c.
1154   6000–3000 BC): growth and collapse of decentralised networks. In *Surplus without the state, political
1155   forms in prehistory, 10th archaeological conference of Central Germany, October 19-21, 2017 in Halle
1156   (Saale)*.
1157   Wang, J., Song, C., Reager, J. T., Yao, F., Famiglietti, J. S., Sheng, Y., ... & Wada, Y. (2018). Recent global
1158   decline in endorheic basin water storages. *Nature geoscience*, *11*(12), 926-932.
1159   Wierik, S. A., Cammeraat, E. L., Gupta, J., & Artzy-Randrup, Y. A. (2021). Reviewing the impact of land use
1160   and land-use change on moisture recycling and precipitation patterns. *Water Resources Research*, *57*(7),
1161   e2020WR029234.
1162   Williams, M. (2003). *Deforesting the earth: from prehistory to global crisis*. University of Chicago Press.
1163   Wright, D. K. (2017). Humans as agents in the termination of the African Humid Period. *Frontiers in Earth
1164   Science*, *5*, 237134.
1165   Wunderling, N., Staal, A., Sakschewski, B., Hirota, M., Tuinenburg, O.A., Donges, J.F., Barbosa, H.M.J., &
1166   Winkelmann, R. (2022). Recurrent droughts increase risk of cascading tipping events by outpacing
1167   adaptive capacities in the Amazon rainforest, *Proc. Natl. Acad. Sci. U.S.A.* 119 (32) e2120777119.
1168   Yamanaka, M. D., Ogino, S. Y., Wu, P. M., Jun-Ichi, H., Mori, S., Matsumoto, J., & Syamsudin, F. (2018).
1169   Maritime continent coastlines controlling Earth's climate. *Progress in Earth and Planetary Science*,
1170   *5*(1), 1-28.
1171   Yang, Y., Roderick, M. L., Guo, H., Miralles, D. G., Zhang, L., Fatichi, S., ... & Yang, D. (2023).
1172   Evapotranspiration on a greening Earth. *Nature Reviews Earth & Environment*, *4*(9), 626-641.
1173   Zhang, X., Zhang, L., Zhao, J., Rustomji, P., & Hairsine, P. (2008). Responses of streamflow to changes in
1174   climate and land use/cover in the Loess Plateau, China. Water Resources Research, 44(7).
1175   Zeng, J., Zhang, Q. (2020). The trends in land surface heat fluxes over global monsoon domains and their
1176   responses to monsoon and precipitation. *Sci Rep* 10, 5762.